

1-1-2009

Conventional frequency ultrasound detection of tumor response in vivo to cancer treatment administration

Naum Papanicolau
Ryerson University

Follow this and additional works at: <http://digitalcommons.ryerson.ca/dissertations>

 Part of the [Electrical and Computer Engineering Commons](#)

Recommended Citation

Papanicolau, Naum, "Conventional frequency ultrasound detection of tumor response in vivo to cancer treatment administration" (2009). *Theses and dissertations*. Paper 907.

RC
570.3
D53
P37
2009

CONVENTIONAL FREQUENCY ULTRASOUND
DETECTION OF TUMOR RESPONSE *IN VIVO* TO
CANCER TREATMENT ADMINISTRATION

by

Naum Papanicolau, B.Sc.

Ryerson University,

Toronto, Ontario, Canada 2006

A thesis presented to Ryerson University in partial
fulfillment of the requirements for the degree of

Masters of Applied Science

in the program of

Electrical and Computer Engineering

Toronto, Ontario, Canada, 2009

©Naum Papanicolau 2009

CONVENTIONAL FREQUENCY ULTRASOUND DETECTION OF TUMOR RESPONSE *IN VIVO* TO CANCER TREATMENT ADMINISTRATION

Naum papanicolau,

MSc. Electrical and Computer Engineering

Ryerson University, 2009

Abstract

Current methods employed to evaluate patient response to cancer therapy are typically invasive requiring examination of excised tissue. The development of a non-invasive method of monitoring patient response to cancer therapy administration would potentiate clinical decisions permitting clinicians to adjust therapy regimens early in a treatment course based upon individual patient responses. It has been previously demonstrated that high frequency ultrasound is capable of reliably quantifying structural changes in tumor morphology in response to cancer therapies. Preliminary work has also indicated that ultrasound employed at clinically relevant frequencies (1-15 MHz) can detect apoptotic cell death using *in vitro* models. This thesis examines changes in tumor morphology in response to cancer therapy administration employing ultrasound at a clinically applicable frequency in a preclinical *in vivo* mouse model. The power spectrum of the radiofrequency data obtained from tumors was analyzed via linear regression spectroscopic analysis, as well as evaluating a statistical analysis of the amplitude distribution of the signal envelope. It is demonstrated here for the first time that 7 MHz ultrasound can detect apoptotic and other forms of cell death *in vivo*. A potential for a parametric imaging technique to visually represent analysis results is also demonstrated.

I hereby declare that I am the sole author of this thesis.

I authorize Ryerson University to lend this thesis or dissertation to other institutions or individuals for the purpose of scholarly research.

I further authorize Ryerson University to reproduce this thesis by photocopying or by other means, in total or in part, at the request of other institutions or individuals for the purpose of scholarly research.

Acknowledgments

I would like to acknowledge the support of all those who helped and supported me through the years of this research. I would like to acknowledge my supervisor Dr. Alireza Sadeghian for providing me the opportunity to continue my education and reach my goals and without whose support I would not have been able to accomplish this work.

I would also like to acknowledge and thank Dr. Gregory Czarnota for allowing me to conduct research in his laboratory at Sunnybrook Health Sciences Centre. It was an amazing opportunity which does not come often in life and I am grateful for having the privilege to be a part of the research team.

Additionally, I would like to thank all the members of the Czarnota lab team who have provided me guidance and assistance through the years. It is sincerely appreciated.

Contents

| | |
|--|-----|
| Abstract | ii |
| Acknowledgments | iv |
| List of Figures | vii |
| List of Symbols | xii |
| Chapter 1 Background and Introduction. | 1 |
| 1.1 Benefits of Ultrasound | 1 |
| 1.2 Ultrasound Imaging | 2 |
| 1.3 Ultrasound Scattering Properties | 3 |
| 1.4 Ultrasound Tissue Characterization | 8 |
| 1.4.1 Spectral Analysis in Tissue Characterization | 8 |
| 1.4.2 Statistical Analysis in Tissue Characterization. | 11 |
| 1.5 Experimental Analysis Methods | 14 |
| 1.5.1 Spectral Analysis | 14 |
| 1.5.2 Statistical Analysis | 17 |
| 1.5.2.1 PDF Parameter Estimations | 17 |
| 1.5.2.2 Direct Statistical Measurements | 19 |
| 1.6 Research Motivation | 21 |
| 1.7 Contributions | 23 |
| Chapter 2 Experimentation | 24 |
| 2.1 Background and Introduction | 24 |
| 2.2 Materials and Method | 27 |

| | |
|---|----|
| 2.2.1 Experimental Design and Data Collection | 27 |
| 2.2.2 Analysis Methods | 29 |
| 2.3 Results | 33 |
| 2.4 Discussion | 38 |
| Chapter 3 Conclusion and Future work | 41 |
| Appendix | 46 |
| A.1 Experimental Design | 46 |
| A.2 Data Collection | 46 |
| A.3 Data Analysis | 47 |
| A.4 L14-5/38 Transducer Characterization | 48 |
| Figures | 50 |
| References | 63 |

List of Figures

1. High frequency ultrasound images of acute myeloid leukemia cells and corresponding TUNEL stained light microscopy images. Acute myeloid leukemia cells have been exposed to the chemotherapeutic agent cisplatin for 0, 6, 12, 24 and 48 hours (left to right panel, respectively). The increase in cell echogenicity correlates with maximal apoptotic response at 24 hours. Lookup table colour bar corresponds to pixel values of 0 on the left and the right the color corresponding to a pixel value of 256. Image reproduced from Czarnota *et al.* [Ultrasound biomicroscopy of viable, dead and apoptotic cells. *Ultrasound in Med and Biol.* 1997: Vol. 23 pp 961-965]
2. Backscatter intensity measurements of acute myeloid leukemia cell populations with varying concentrations of apoptotic cells. Increases in backscatter amplitude measurements correlate with increasing apoptotic elements peaking at a 40% - 80% concentration within the population. Figure reproduced from Czarnota *et al.* [unpublished results]
3. Ultrasound image of human head and neck tumor with corresponding histology and parametric images. Top left shows an ultrasound B-mode image and right corresponding TUNEL-stained image indicating an area of cell death of similar shape as the hyper-echoic area in the ultrasound image and parametric images computed from the local estimates of ultrasound integrated backscatter (UIB), spectral intercept (SI), and spectral slope (SS). The color-bars under each parametric image indicate the ranges of the corresponding estimates of the spectral parameters. Figure reproduced from Vlad *et al.* [Quantitative ultrasound

characterization of response to radiotherapy in cancer mouse models. Clin Cancer Res 2009: pp 2067 - 2075]

4. Ultrasound B-mode image overlaid with a parametric image of the GG a parameter from a NHL tumor before treatment (left) and 12 hours post treatment (right). Figure reproduced from Tunis *et al* [Monitoring structural changes in cells with high frequency ultrasound signal statistics. Ultrasound in Med and Biol. 2005: Vol. 21 pp 1041-1049].
5. Power spectra obtained from water indicating the system noise detected by the employed transducer (bottom) and from an agar embedded glass bead phantom (top).
6. Representative normalized power spectra obtained using high frequency ultrasound from PC3 tumor administered microbubble anti-vascular therapy followed by 8 Gy X-ray radiation treatment (top). Power spectra shown from the reference pulse, region of interest, and corresponding normalized spectra with best fit line from top to bottom, respectively. Representative normalized power spectra obtained using low frequency ultrasound from PC3 tumor administered microbubble anti-vascular therapy followed by 8 Gy X-ray radiation treatments (middle). Power spectra shown from the reference pulse, region of interest and corresponding normalized spectra with best fit line, from top to bottom, respectively. Normalized power spectra from low and high frequency data and corresponding best fit line within a -6 dB window (bottom).
7. Pictorial representation of frequency window determination corresponding to a -6 dB bandwidth.

8. A sample radiofrequency line, with its corresponding envelope, and the histogram of the envelope amplitude, normalized to an area of one. Reproduced from Tunis *et al* [33].
9. Ultrasound B-mode images reconstructed from radiofrequency data with region of interest selection for low and high frequency data on the left and right, respectively. The horizontal line indicates the transducer focus.
10. Representative data from untreated, 8 Gy X-ray, anti-vascular microbubble and anti-vascular microbubble followed by 8 Gy X-ray treatment administration groups, from left to right, respectively. Representative 7 MHz ultrasound B-mode images of PC3 tumors demonstrating increases in tissue echogenicity with treatment administration in contrast to untreated tumor (first row). Representative normalized power spectra obtained from PC3 tumors prior to treatment and at 24 hours following treatment administration (second row). Low magnification light microscopy images of TUNEL stained PC3 tumors (third row). Light microscopy images of hematoxylin and eosin stained tumor slices obtained at high magnification (fourth row). Distribution of cell versus nucleus size measurements representing morphology of responsive regions within the tumor (fifth row).
11. (A) Mid-band $\text{fit}\Delta$ results for high and low frequency data in the four treatment groups. (B) Spectral slope Δ results for high and low frequency data in the four treatment groups. (C) Zero-MHz intercept Δ results for high and low frequency data in the four treatment groups. Blue bars represent low frequency data and red bars represent high frequency data.

12. (A) Rayleigh $\sigma\Delta$ results for high and low frequency data in the four treatment groups. (B) Mean Δ results for high and low frequency data in the four treatment groups. (C) Skewness Δ results for high and low frequency data in the four treatment groups. (D) Kurtosis Δ results for high and low frequency data in the four treatment groups. Blue bars represent low frequency data and red bars represent high frequency data.
13. (A) Gamma shape parameter Δ results for low frequency data from the four treatment groups. (B) Gamma scale parameter Δ for low frequency data from the four treatment groups. (C) Generalized Gamma $c/v\Delta$ for high frequency data from the four treatment groups. (D) Generalized Gamma $\alpha\Delta$ for high frequency data from the four treatment groups.
14. Low frequency ultrasound signal envelope amplitude distribution histogram with Rayleigh and Gamma PDF estimations from untreated and microbubble followed by X-ray radiation treated PC3 tumor (A and B, respectively). High frequency ultrasound signal envelope amplitude distribution histogram with Rayleigh and Generalized Gamma PDF estimations from untreated and microbubble followed by X-ray radiation treated PC3 tumor (C and D, respectively).
15. Low frequency ultrasound B-mode images of sample wells containing acute myeloid leukemia cells (top) and region of interest selection (second from top). The left well contains untreated cells and the right well contains cells exposed to the chemotherapeutic agent cisplatin for a 12 hour period. The third image from the top displays parametric image overlays employing a region segmentation algorithm. The bottom image displays parametric image overlays employing a

sliding window algorithm. The parametric scale bar corresponds to mid-band fit values of of -100 dBr on the left and 0 dBr on the right.

16. Representative low frequency ultrasound B-mode images with parametric overlay. Parametric images were computed using a sliding window algorithm within a ROI. The top row presents data obtained from tumors prior to treatment and the bottom data collected from tumors 24 following treatment administration. Treatment administration consisted of anti-vascular microbubble alone, 8 Gy X-ray radiation and anti-vascular microbubble and 8 Gy X-ray radiation combination treatments from left to right respectively. The parametric scale bar corresponds to mid-band fit values of of -100 dBr on the left and 0 dBr on the right.

List of Symbols

α – Generalized Gamma scale parameter

α – Attenuation coefficient

Θ – Scattering angle [rad]

λ – Wavelength [m/Hz]

σ – Rayleigh parameter

A – Signal Attenuation [dB/cmMHz]

C – Speed of sound [m/s]

c – Generalized Gamma shape parameter

d – Distance [m]

d_n – Boundary coefficient

dB – Decibels

dBr – Decibels relative to reference

f – Frequency [Hz/s]

h – Histogram bin size

k – Compressibility

K – Wavenumber [m^{-1}]

R – Backscatter signal amplitude

ρ – Density [kg/m^3]

P_n – nth order Legendre polynomial

v – Generalized Gamma shape parameter

Z – Acoustic Impedance [kg/m^2c]

Chapter 1 – Background and Introduction

1.1 Benefits of ultrasound

There are many imaging modalities which are currently employed in clinical settings. It has been shown that several of these imaging technologies may possess the capacity to monitor changes in tissue microstructure in relation to cancer treatment administration. Technologies which have been examined to detect tumor treatment response include fluoro-2-deoxy-D-glucose positron emission tomography (PET) in addition to magnetic resonance imaging (MRI) [1]. Although it has been demonstrated that these imaging modalities may be employed in the detection of tumor response, they do not possess the unique qualities afforded by ultrasound.

Ultrasound imaging is used widely in many clinical applications throughout the world accounting for near 25% of all medical imaging [2]. It has been demonstrated through several decades of study and application that ultrasound is a technology which can be safely used on a routine basis. Since ultrasound does not employ ionizing radiation nor induce significant thermal effects when applied in a clinically acceptable manner, it may be frequently employed without concern of bioeffects to patients. Ultrasound devices are typically compact and mobile whereas the imaging modalities mentioned above do not possess this quality, significantly reducing the range of accessible patients which can be monitored for treatment effects. Additionally, ultrasound technology benefits from being cost effective, as equipment is relatively inexpensive when compared to alternative imaging modalities. Overall, ultrasound imaging provides a safe, mobile, and

inexpensive technology thus making it an excellent candidate for the purpose of monitoring patient response to cancer therapy in a clinical setting.

1.2 Ultrasound Imaging

The use of acoustic waves, and specifically ultrasound, has widespread applications in modern technology. The use of acoustic waves has been employed in a wide range of military and civilian applications over a period of many decades. Examples of the use of acoustic waves being employed to monitor physical properties of materials can be seen in applications such as the military development of SONAR (Sound Navigation And Ranging) to locate underwater objects and in the detection of flaws in metal castings [3]. Ultrasound imaging works in a similar manner to these technologies by generating an acoustic wave and obtaining information from echoes received from that wave from its interactions with the propagating medium.

The majority of ultrasound imaging is conducted in what is known as pulse-echo mode. This imaging method employs an acoustic pulse which is propagated longitudinally through a given medium. Interactions of the acoustic pulse and the propagation medium cause reflections of the pulse back to the source which is used to generate the image. This results in what is known as ultrasound amplitude mode (A-mode) imaging which generates an image based upon the intensity of the reflected wave versus time. The depth of the reflection source is calculated given the speed of sound within the propagating medium and the amount of time required for the reflection to return to the source. The most commonly employed ultrasound imaging modality employs this concept and displays information regarding the brightness related to the echo signal amplitude.

Conducting multiple A-mode scans through the investigating medium allows for a two dimensional B-mode image to be created.

1.3 Ultrasound Scattering Properties

Ultrasound imaging is based upon the interaction of an acoustic wave and the given medium through which it propagates. Interactions of the pulse and the tissue medium cause a proportion of the ultrasound wave to be reflected back toward the source allowing for an image to be generated. The reflected acoustic wave is known as a backscatter signal, which is dependent upon properties of the source of the reflection (known as the scatterer) as well as properties of the ultrasound wave itself. Properties of scattering sources which affect the backscatter signal are the size, physical and number density, compressibility and the distribution of the scatterers within the medium.

There is a direct relationship between the wavelength of the acoustic wave, the size of the scatterer and the resulting backscatter signal. When a scattering source is much larger than the ultrasonic wavelength, the interaction between the wave and the source can be approximated by that of a flat surface. In this scenario, the wave is reflected 180° possessing an amplitude determined by a property of the scattering source known as the reflection coefficient. The reflection coefficient itself is dependent upon a property of materials known as acoustic impedance, which is based upon the density of a material

and the speed at which the ultrasound wave is propagating as shown in:

$$Z_n = \rho_n c_n \quad (1.1)$$

where ρ_n is the density of the medium and c_n the speed of the ultrasound wave. Given this property, the reflection coefficient for 180° reflection is determined by:

$$R = \frac{Z_2 - Z_1}{Z_2 + Z_1} \quad (1.2)$$

where Z_1 and Z_2 are the acoustic impedance of the surrounding medium and the scattering source respectively.

A second type of ultrasound scattering is found when the incident wave has a wavelength similar to the size of the source scatterer. This scattering interaction occurs between ultrasound pulsed at high frequencies and human tissue, as the resulting wavelength is of the same size to that of cells and their nuclei. This type of scattering is referred to as Faran or Mie scattering, a naming convention typically in reference to the scattering of electromagnetic radiation by a sphere, the acoustic solution to which was derived by Faran [4,5]. The amplitude of the backscatter signal in Mie-type scattering is given by:

$$R = \sum_{n=1} d_n (J_n - iY_n) \left(\frac{2\pi f}{c} \right) P_n (\cos \theta) \quad (1.3)$$

where P_n is the n^{th} order Legendre polynomial, and θ is the angle relative to the incident wave, J_n and Y_n are Bessel functions of the first and second kind respectively, and d_n is a coefficient determined for the boundary conditions between the sphere and surrounding medium.

A third type of ultrasound scattering occurs when the scattering source is much smaller than the wavelength of the incident ultrasound wave. This type of scattering is known as Rayleigh scattering and is typically found in the interaction between ultrasound waves employed at clinically relevant frequencies and tissue. At frequencies below 15 MHz which is typically used in clinical settings, the wavelength of the ultrasound pulse is on the order of hundreds of microns, considerably larger than the tens of microns found in typical tissue cellular structures.

The reflected wave was first described by Lord Rayleigh [7]:

$$R(r, \theta) \approx e^{-1K_1 r} \frac{k_1^2 a^3}{3r} \left[\frac{K_2 - K_1}{K_1} + \frac{3(\rho_2 - \rho_1)}{2\rho_2 + \rho_1} \cos \theta \right] \quad (1.4)$$

where subscript 1 denotes the properties related to the surrounding medium and subscript 2 the scatterer, ρ is the density, a the scatterer diameter, r the distance from the scatterer and θ the angle relative to the incident wave. The compressibility k and wave number K are given by equations:

$$K_n = \frac{1}{p_n c_n^2} \quad (1.5)$$

$$k_n = \frac{2\pi f}{c_n} \quad (1.6)$$

Where n is 1 or 2 for the surrounding medium of scatterer, p is the density, c is the speed of sound and f frequency.

For very small scatterers ($a \ll \lambda$) and Rayleigh scattering, the backscatter echo signals depend upon:

- 1) The number of scatterers per unit volume
- 2) The acoustic impedance changes at the scatterer interfaces
- 3) The size of the scatterers (scattering increases with increasing radius)
- 4) The ultrasound frequency (scattering usually increases with increasing frequency for very small scatterers with intensity proportional to frequency raised to the fourth power) [6].

Given the differences in how ultrasound interacts with scattering sources relative to the wavelength of the employed pulse, the frequency employed determines the manner in which the backscatter signal will be generated. This is due to the fact that there is a direct relationship between the ultrasonic frequency and the wavelength of the resulting wave given by equation:

$$\lambda = \frac{c}{f} \quad (1.7)$$

Where λ is the wavelength, c is the velocity of the propagating wave within the given medium and f the frequency. This results in an inverse relationship between the ultrasound frequency and the resulting wavelength, with the wavelength decreasing with increasing ultrasound frequencies.

The aim of this thesis is to investigate the potential of ultrasound to detect structural changes in tissue microstructure in response to cancer treatment administration

employing clinically relevant frequencies. The foundation to this study is primarily based upon research conducted employing frequencies above that of clinical use. That body of work shows strong evidence that ultrasound frequencies above 20 MHz can be employed to reliably detect changes in relation to cancer therapy administration which we hypothesize to be related to changes in cellular structure [8-13]. Unfortunately, this is not generally applicable in a clinical manner as the penetration depth at these frequencies is not sufficient for many clinical applications. This is due to ultrasound attenuation as it propagates through tissue. Attenuation is the loss of signal intensity as it passes through a medium, and is described by:

$$A = \alpha df \quad (1.8)$$

where A is the attenuation of the signal, α is the material frequency dependant attenuation coefficient (dB/MHz*cm), d the distance into the medium and f the employed frequency. This means that there is an increase in the amount of signal attenuation proportional to the frequency employed. As such, lower ultrasonic frequencies are capable of penetrating deeper into tissue enabling their use in clinical applications.

Although the use of ultrasound at conventional frequencies does permit significantly increased tissue penetration, there is a substantial difference in the resulting wavelength. As the wavelength is considerably larger than that found in higher frequencies, the interaction between the ultrasonic pulse and the cellular medium falls closer into the realm of Rayleigh scattering. It was previously unknown if the use of ultrasound at these frequencies would be sufficiently affected by the changes in cellular microstructure in response to treatment. Initial investigations conducted using *in vitro* models did indicate

the potential for the detection of cell death [25], however previous to this work there has not been an attempt to ascertain the potential of ultrasound for treatment monitoring at clinically relevant frequencies in an *in vivo* model.

1.4 Ultrasound Tissue Characterization

Conventional applications of ultrasound imaging are widespread permitting the clinical visualization of internal anatomical features. Although extremely useful in many clinical settings, the standard use of ultrasound B-mode imaging does not provide quantitative information regarding tissue microstructure nor provide the ability to distinguish between various tissue types other than the differentiation of gross anatomical structures. Through analysis of the ultrasound backscatter signal, quantitative ultrasound techniques have been developed employing ultrasound waves to characterize tissue. These techniques of ultrasound tissue characterization used in this study generally fall into two classes, the first of which examines the frequency distribution of the power spectrum in order to derive acoustic properties, and the second examining statistics of the signal envelope amplitude distribution.

1.4.1 Spectral Analysis in Tissue Characterization

Analysis of the power spectrum obtained from backscatter signals has been employed in a variety of tissue characterization applications. The intensity and frequency distribution of the backscatter signal has been shown to be related to features of tissue micro-structure specifically in the size, distribution and acoustic properties [14, 15]. The use of

quantitative ultrasound techniques for characterizing tissue has been employed in applications such as distinguishing areas of malignancy in the human prostate [16, 17] and in the differentiation of liver as well as cardiac abnormalities [18, 19]. Spectroscopic analysis techniques have also been employed to differentiate between benign fibroadenomas from mammary carcinomas and sarcomas [20].

The use of tissue characterization in detecting changes in tissue morphology in relation to cancer therapy administration was initiated by the work of Czarnota and Kolios *et al* employing high frequency ultrasound [8]. That research began with the discovery that Acute Myeloid Leukemia (AML) cells present an increase in echogenicity when exposed to the chemotherapeutic agent cisplatin. As demonstrated in Figure 1, it was observed that backscatter from AML cells exposed to cisplatin increased with drug exposure periods which histologically correlated to increasing levels of apoptotic cell death. This phase of research employed drug exposure-time dependant experimentation, in addition to concentration dependant experiments which analyzed populations of cells containing various concentrations of viable and apoptotic cells. Figure 2 demonstrates the observed relation between the concentration of a population containing cells undergoing apoptosis, and the corresponding observed increase in ultrasound backscatter intensity.

Although initial investigations were based upon quantification of B-mode image intensity measurements, the work progressed into quantitative ultrasound measurements of the normalized power spectrum. That work confirmed that ultrasound tissue characterization employing spectroscopic analysis was capable of quantifying changes in microstructure again in an *in vitro* AML cell model [13, 21]. Observed measurements of the mid-band fit and spectral slope parameters indicated a maximal 25-fold increase in backscatter

intensity with spectral slope increases histologically correlated to decreases in cell and nucleus size.

Subsequent to these initial studies, research in the use of quantitative ultrasound as a tool for tissue characterization progressed into *in vivo* experimentation. Work done by several researchers [22-24] has confirmed that the techniques employed in the high frequency analysis of *in vitro* models are capable of detecting changes in the tissue micro-structure of tumors exposed to a variety of cancer therapies *in vivo*. These studies have encompassed a wide variety of tumor cell lines and therapy administrations in addition to “time-course” studies. High frequency analysis has demonstrated significant increases in backscatter intensity in addition to changes in spectral slope than can be histologically correlated to cell death of tumors in response to treatment administration. Figure 3 shows a high frequency ultrasound image of a human head and neck tumor mouse xenotransplant treated with radiotherapy and an associated TUNEL-stained slice of the same tumor. It is evident that areas of the tumor indicating significant levels of apoptotic response in histopathology demonstrate significantly higher levels of tissue echogenicity. Spectral quantification techniques have been employed in the generation of parametric images indicating ultrasound quantification techniques employed at high frequencies capable of measuring and distinguishing regions of response from otherwise viable tumor tissue.

Initial investigation into the efficacy of ultrasound employed at a clinically relevant frequency (10 MHz) in the detection of micro-structural changes in tissue as a result of cancer therapy has been conducted by Azrif *et al* in an *in vitro* AML cell model [25]. Similar to the initial work done by Czarnota and Kolios *et al* that study examined both

cisplatin time exposure and apoptotic cell concentration dependence in experiments. Employing spectroscopic analysis of the normalized power spectra, that proof of principle investigation observed significant increases in mid-band fit and spectral slope histologically correlated to apoptotic cell death.

1.4.2 Statistical Analysis in Tissue Characterization

The analysis of statistics derived from the amplitude distribution of signal envelope obtained from the ultrasound backscatter signal has also been used as a method of classifying tissue. This is possible due to the relationship of scatterer properties and the statistical distribution of the amplitude of the signal envelope. Theoretical models relating the statistics of the signal envelope and scatterer properties have been developed with several *in vivo* studies corroborating the feasibility of this technique [26-29]. Work done by Shankar *et al* has shown the use of signal statistics in the characterization of benign and malignant breast tumors [30, 31]. This technique has also been employed in the differentiation of reperfused myocardium from infarcted tissue as well as in the differentiation of various skin types [32].

Tunis *et al* investigated the use of signal statistics in the detection of changes in tissue micro-structure in response to cancer therapy administration [10]. This work employed high frequency ultrasound and encompassed theoretical modelling, *in vitro* studies of AML cells in addition to *in vivo* experimentation. Employing probability density function estimations of signal envelope amplitude based histograms, that work demonstrated a relationship between measured changes in amplitude distribution and changes in tissue microstructure in response to treatment administration. It was found that statistical analysis of high frequency ultrasound backscatter signals was highly

sensitive to structural changes in cells with observed sensitivity to changes within as little as 2.5% of cells within an otherwise viable population. Good correlation was shown between theoretical models and experimental observation in both *in vitro* and *in vivo* models. Similar to the parametric imaging generated by Vlad *et al* employing spectral analysis, Tunis showed initial evidence that statistics of the signal envelope can be used as a tool to visualize response [22, 33]. As shown in Figure 4, parametric images of analysis regions from treated and untreated tumors generated employing the Generalized Gamma a parameter are capable of visually representing increases in tissue echogenicity. That initial imaging technique did lay the groundwork for the future examination of the capacity of signal envelope statistic analysis as a method of non-invasively quantifying and displaying the effects of cancer therapies.

The research described in this section represents background information for the work done in this thesis. It has been demonstrated that a substantial body of research exists indicating the ability of ultrasound as an imaging modality capable of quantifying micro-structural characteristics of tissue. The use of ultrasound at high frequencies has been examined in depth as a method of detecting changes in tissue micro-structure in response to cancer treatment administration. Examination of high frequency ultrasound employing both spectroscopic analyses as well as statistical analysis of the amplitude distribution of the signal envelope obtained from backscatter signals has been demonstrated to be acutely sensitive to cell death in theoretical, *in vitro* and *in vivo* cell models. Initial investigations into the efficacy of conventional frequency ultrasound as a method of cell death detection conducted employing spectroscopic analysis found good correlations between the capabilities of ultrasound at high and conventional frequencies. Given this

positive initial foray into conventional frequency ultrasound, this thesis aims to show that this imaging modality has the capacity to detect changes in tissue micro-structure in response to cancer therapy in an *in vivo* pre-clinical model.

1.5 Experimental Design and Analysis

1.5.1 Spectral Analysis

Analysis of experimental data was conducted via examination of the frequency distribution obtained for the backscatter signal. The power spectrum of the signal provides information regarding the distribution of the power in the backscatter signal in relation to the frequency range. The power spectrum was calculated employing the fast Fourier transform function in the Matlab environment. This algorithm computes the Fourier and inverse Fourier transform pair employing:

$$X(k) = \sum_{j=1}^N x(j) \omega_N^{(j-1)(k-1)} \quad (1.9)$$

$$x(j) = \left(\frac{1}{N}\right) \sum_{k=1}^N X(k) \omega_N^{-(j-1)(k-1)} \quad (1.10)$$

where N is the length of the vector and ω the N th root of unity described by:

$$\omega_N = e^{(-2\pi i)/N} \quad (1.11)$$

The resulting power spectrum was obtained from the logarithmically compressed vector of the absolute value of the squared FFT function employed. In order to calculate the power spectrum for an entire analysis region, the power spectrum was calculated for each individual scan line through the selected region and subsequently averaged using:

$$PS(x) = \frac{\sum_{i=1}^N x_i}{N} \quad (1.12)$$

where x represents the position along the power spectrum vector (i.e. the frequency) and N represents the number of scan lines through the selected region on analysis.

Having computed the power spectrum for the analysis region, the data was subsequently normalized using a calibration pulse. Calibration pulse normalization was used to remove the effects of system transfer functions from the obtained signal. As the power spectrum was manipulated once in logarithmically compressed form, normalization was obtained from the subtraction of the two spectra according to:

$$NPS(x) = PS(x) - R(x) \quad (1.13)$$

where x represents the position along the normalized power spectrum vector, PS is the power spectrum of the analysis region and R the spectrum of the calibration pulse.

Linear regression analysis of the normalized power spectrum was calculated employing a -6 dB window determined from the peak in the reference spectrum. The window size is commonly employed as this is the realm in which a majority of the power and useful information is contained within the signal. Figure 7 displays a pictorial representation of how the window was determined for the calculation of the corresponding frequency range.

Having calculated the normalized power spectrum and the frequency range corresponding to the 6dB window, linear regression was applied in order to obtain a best fit line. This was accomplished using a polynomial fitting curve implemented in Matlab as `polyfit()` which employs:

$$p(x) = p_1x^n + p_2x^{n-1} + \dots + p_nx + p_{n+1} \quad (1.14)$$

This function returns the coefficients of a polynomial $p(x)$ of degree n that fits the data in a least squares sense. In this case the degree which was employed was 1.

Figure 6 depicts the process of power spectrum normalization. The topmost graph represents the averaged power spectrum obtained from a region of interest, the middle chart represents the power spectrum from a reference pulse employed in normalization and the bottom graph represents the resulting normalized power spectrum with the best fit line within the calculated 6 dB window. Parameters of the normalized power spectrum investigated in this study are the mid-band fit, the spectral slope and 0-MHz intercept. The mid-band fit is defined as the point on the best fit curve at the centre of the employed bandwidth. This parameter provides an indication of backscatter intensity and has been correlated to scatterer properties relating to the size, shape, distribution and acoustic impedance of the scatterer. The spectral slope is the slope of the linear regression line within the analysis window and is related to the size of the scattering source and the attenuation in the medium. The 0-MHz intercept is the amplitude of the best fit line extended to the 0-MHz point and is related to the concentration of scatterers within the tissue as well as the strength of the scatterers [34].

1.5.2 Statistical Analysis

The second type of analysis conducted in this study was based upon a statistical evaluation of the amplitude distribution contained in the signal envelope. Statistical analysis was conducted in two manners, the first by fitting experimental data to a probability density function and the second by examining the amplitude distribution of the signal envelope. In order for this analysis to be conducted, the signal envelope needed to be obtained from the radiofrequency data. This was accomplished by taking the absolute value of the Hilbert transform of the radiofrequency signal.

1.5.3 Probability Density Function Parameter Estimations

Statistical analysis of the signal envelope was conducted through the use of probability density function parameter estimations. Amplitude data of the signal envelope was initially employed to generate a histogram depicting the distribution of backscatter amplitudes within the region of interest. Histograms bin sizes were determined using equation 1.15 developed by Scott [35]:

$$h_n = 3.49sn^{-1/3}, \quad (1.15)$$

where h_n is the optimal bin size and sn the standard deviation of the data set. This method of histogram generation ensured that each individual analysis set was computed with a bin size depicting the distribution of the data within the set. Figure 8 depicts the generation of the signal envelope from the radiofrequency data and the associated histogram employing the optimal bin size algorithm [10].

In order to fit probability density functions to the associated histogram, the maximum likelihood estimation (MLE) was employed. The Matlab MLE function employs the Nelder-Mead Simplex method in order to maximize the likelihood of obtaining a set of n values $(r_1 \dots r_n)$ with a distribution by modifying the distribution parameters. This study investigated the potential fitting accuracy of three probability density functions, namely the Rayleigh, Gamma and Generalized Gamma distributions.

Equation 1.16 shows the likelihood function employed for the Rayleigh PDF:

$$\hat{\sigma}^2 = \frac{\langle r^2 \rangle}{2}, \quad (1.16)$$

where $\langle \rangle$ indicates the mean of the value for n values (r_1, \dots, r_n) .

Equation 1.17 shows the likelihood function employed for the Gamma PDF:

$$L(k, \theta) = \prod_{i=1}^N f(x_i; k, \theta), \quad (1.17)$$

where k represents the shape parameter and θ the scale parameter and $f(x_i; k, \theta)$ represents the Gamma PDF given by:

$$f(x_i; k, \theta) = x^{k-1} \frac{e^{-\frac{x}{\theta}}}{\theta^k \Gamma(k)}, \quad (1.18)$$

Where $\Gamma(k)$ is defined by:

$$\Gamma(k) = (k - 1)! \quad k > 0. \quad (1.19)$$

The likelihood function employed in the generalized gamma distribution was implemented by Tunis, and is defined by:

$$L(c, v, a) = \prod_{i=1}^n p(r_i; c, v, a) \quad (1.20)$$

where $p(r_i; c, v, a)$ is Generalized Gamma PDF defined by:

$$p(r_i; c, v, a) = \frac{2sv^v r^{2ms-1}}{\Gamma(v)\Omega^m} e^{-\left(\frac{m}{\Omega}\right)r^{2s}} \quad (1.21)$$

where $c = 2s$ and $\Omega = va^c$.

1.5.4 Direct Statistical Measurements

In addition to statistical measurements based upon probability density function parameter estimations, other statistical parameters of the signal envelope were calculated. These parameters include the mean, skew and kurtosis of the amplitude distributions.

The mean is a direct measurement of the average amplitude within a given data set. Since the amplitude of the envelope is directly related to the intensity of the backscatter signal, this parameter provides a measurement of the average intensity of the ultrasound backscatter. The mean value of the signal envelope was calculated using:

$$Mean(x_1 \dots x_N) = \frac{\sum_{i=1}^N x_i}{N}, \quad (1.22)$$

where N represent the number of values within the given vector.

The skewness of the distribution was measured in order to quantify changes in the symmetry of the distribution in relation to treatment administration. An increase in the skew parameter indicates an increase in the proportion of the data to the right of the distribution peak.

Skewness is known as the third standardized moment about the mean and is defined by:

$$\gamma(x_1 \dots x_n) = \frac{\frac{1}{n} \sum_{i=1}^n (x_i - \bar{x})^3}{\left(\frac{1}{n} \sum_{i=1}^n (x_i - \bar{x})^2\right)^{3/2}}, \quad (1.23)$$

where \bar{x} represents the samples mean derived from equation 1.22.

In addition to the mean and skewness measurements, an analysis of the kurtosis of the signal envelope was conducted. Kurtosis is a parameter which measures the relative height of the peak of the distribution when compared to the tail ends. Kurtosis is known as the fourth standard deviation about the mean and is defined by:

$$g(x_1 \dots x_n) = \frac{\frac{1}{n} \sum_{i=1}^n (x_i - \bar{x})^4}{\left(\frac{1}{n} \sum_{i=1}^n (x_i - \bar{x})^2\right)^2} \quad (1.24)$$

where \bar{x} is the sample mean derived from Equation 1.22.

Increasing values of the kurtosis parameter indicate that a larger portion of the variance within a dataset is due to deviations larger than that of the standard deviation. These larger deviations in comparison to the data set can be found at the right and left ends of the distribution indicating either larger or smaller values. In conjunction with skewness measurements which are used to quantify relative shifts in symmetry, is it possible to ascertain the positioning of increases of large deviations within the distribution.

1.6 Research Motivation

The hypothesis of this thesis is that ultrasound employed at clinically applicable frequencies may be employed to detect and quantify the effects of cancer therapy administration in an *in vivo* mouse model. The motivation for this was arrived from a long body of existing research.

It has been previously demonstrated that high frequency ultrasound possesses the capacity to detect micro-structural changes in tissue morphology in response to therapy administration in *in-vitro* and *in vivo* models. This research began with the observation by Czarnota et al. that acute myeloid leukemia cells exhibit increased echogenicity when exposed to the chemotherapeutic agent cisplatin [8]. Quantification of this early research was conducted via examination of voltage values obtained from b-mode ultrasound images. Subsequent analysis was conducted employing spectroscopic analysis techniques analyzing the normalized power spectra obtained from radiofrequency data.

Research into the use of high frequency ultrasound in the detection of cancer treatment administration was further examined employing *in vivo* experimentation. This was conducted employing spectroscopic analysis of the normalized power spectra and observed significant changes in spectral parameters histologically correlated to changes in tissue micro-structure associated with apoptotic cell death [9, 12]. Additional analysis techniques were examined by Tunis, who investigated the use of statistics of the signal envelope in order to quantify changes in ultrasound backscatter as a result of cancer treatment administration [10].

The use of conventional frequency ultrasound in the detection of cancer treatment effects has been previously examined in an *in vitro* acute myeloid leukemia cell model. This

research observed significant changes in spectral parameters histologically correlated to apoptotic cell death. Experimentation employing conventional frequency ultrasound encompassed cell exposure to the chemotherapeutic agent cisplatin for various time periods, in addition to concentration dependant experimentation in which centrifuged samples of viable and apoptotic cells of varying concentrations were analyzed [25]. These experiments observed results similar to those obtained in analysis of high frequency ultrasound backscatter signals providing an initial indication that ultrasound employed at conventional frequencies may be applied in the detection of cancer treatment response. The work in this thesis represents the first time that conventional frequency ultrasound has been employed in an *in vivo* mouse model in the detection of changes in tissue microstructure in response to cancer treatment administration.

1.7 Contributions

The work presented in this thesis represents the collaborative effort of many people in the Czarnota laboratory at Sunnybrook Health Sciences Centre. Contributions of the laboratory members were primarily centered on the experimental setup and data acquisition portions of the research. This includes but is not limited to preparation and injection of tumor cells, tumor treatment administration, ultrasound data acquisition, and the preparation of tumors for histological examination.

During this period I was involved in the experiments being conducted in the laboratory, including several of the aspects mentioned above. My individual contribution to this research however was primarily focused upon the analysis of the acquired data. This included development of software performing spectroscopic and statistical analysis of ultrasound radiofrequency data, in addition to the development parametric image generation to visually represent spectroscopic parameters. Additional work involved quantification of tissue response to treatment administration via analysis of high and low magnification light microscopy image analysis as well as correlation of these results to observations obtained from ultrasound data analysis.

The following chapter provides a detailed overview of experimental setup and design methods in addition to results obtained. It is represented in paper format as it reflects a submission for publication which is to be made in October 2009 to the journal of cancer research.

Chapter 2 - Experiments and Results

2.1 Introduction

The aim of many cancer therapies is to induce cell death within a target tumor in order to destroy it. Current methods of assessing the effects of treatment within a patient during the course of treatment administration are often invasive requiring cytometric analysis of biopsied tissue. A commonly employed clinical assessment is based upon measurement of tumor size, however tumor size reduction often requires several weeks of treatment administration and in some cases tissue diminishment is not present despite a positive treatment response [1]. The advent of a non-invasive manner to monitor patient response to therapy would be advantageous in order to guide the customization of chemotherapy or other cancer therapies. If limited cell death is detected in response to therapy, clinicians would be able to alter an ineffective treatment course to a more efficacious one. In this study, we investigate the potential of quantitative conventional frequency ultrasound to non-invasively monitor the effects of various cancer therapies in real time in an *in vivo* SCID mouse tumor model.

Previous research conducted using high frequency ultrasound (20-50 MHz) assessing its ability to detect changes in tissue microstructure associated with cancer therapies using *in vitro*, *in situ*, and *in vivo* models have indicated its ability to detect cell death [8-13]. Initial observations demonstrated increased tissue echogenicity in acute myeloid leukemia cells exposed to the chemotherapeutic agent cisplatin [8]. Subsequent research employed spectroscopic quantification techniques in addition to statistical analysis of the signal envelope to quantify this effect using high frequency ultrasound in a variety of *in*

vivo and *in vitro* models [8-13]. High-frequency ultrasound has been used to detect effects of photodynamic therapy which induced apoptotic cell death and radiation therapy which induced apoptotic cell death in cases and in other models mitotic arrest. These studies indicated that high frequency ultrasound is sensitive to structural changes associated with cell death with an observed 16-fold maximal increases in backscatter accompanied by increases in spectral slope and 0-MHz intercept. Similar techniques have been employed in a variety of other related ultrasound tissue characterization applications such as in the diagnoses of prostate cancer, liver and cardiac abnormalities and the differentiation of benign fibroadenomas from mammary carcinomas and sarcomas [16-17, 36]. Although high frequency ultrasound (20-50 MHz) benefits from an increased imaging resolution (80-30 μm ultrasonic wavelegths) when compared to clinically utilized frequencies of 1 to 20 MHz (1.5 mm - 80 μm ultrasonic wavelengths), it suffers from a decreased tissue penetration depth limiting its use to animal tumors on superficial sites near the skin surface. The use of clinically employed lower frequencies to detect changes in morphology in response to cell death induced by cancer treatment administration would permit assessing the effectiveness of a significantly increased range of cancer therapies. Benefitting from a substantive increase in tissue penetration capacity, conventional frequency ultrasound may potentially be able to non-invasively monitor the response of patients undergoing therapies for a wide variety of deeper body cancers such as breast and liver malignancies.

Initial investigations into the potential of ultrasound at clinically relevant frequencies in the detection of treatment response were carried out using *in vitro* Acute Myeloid Leukemia (AML) cell models. That work indicated that 10 MHz ultrasound

spectroscopic analysis was able to reliably quantify micro-structural changes histologically correlated with apoptotic cell death in AML cells exposed to the chemotherapeutic agent cisplatin. Experimental design included time-dependant experiments with statistically significant changes in tissue response detection observed within a 6 hour period following drug administration. Additionally, concentration dependant experimentation indicated detection of as little as 2.5% apoptotic cells within an otherwise viable population sample [25]. Parallel data collection employing high frequency ultrasound found good correlation in the detection of response across the employed frequency ranges via spectroscopic quantification of the normalized power spectrum. Other investigations in this range of ultrasound also have indicated that the cell nucleus configuration has a significant influence of high frequency ultrasound backscatter [24].

This study demonstrates for the first time the capacity of conventional frequency ultrasound in quantifying changes in tissue microstructure resulting from cancer therapy administration in an *in vivo* model. In this study we have carried out assessments of ultrasound characteristics of different types of cell death using low-frequency (7 MHz) ultrasound in order to demonstrate the feasibility of using conventional frequency ultrasound to detect cell death. SCID (severe combined immunodeficiency) mice bearing tumors (PC3) were treated in a number of manners to induce different forms of cell death. Animals were exposed to radiation alone to induce mitotic arrest, anti-vascular ultrasound therapy to induce a vascular modulated ischemic apoptotic cell death and a combined treatment of the anti-vascular ultrasound therapy and the radiation which produces an enhanced cell death, in addition to animals which remained untreated. Parallel data was

acquired via high frequency ultrasound. Analysis of both high and low frequency data employed linear regression analysis of the normalized power spectrum in addition to statistical quantification of the signal envelope. Results indicated increases in mid-band fit with the presence of cell death of 5.9 ± 0.92 dB for low-frequency data compared to 6.2 ± 1.15 dB for high-frequency data for samples with prominent cell death. Scattering from untreated animals was invariant, radiation treatment alone resulted in mitotic cell death and spectral slope decrease consistent with mitotic death, whereas vascular treatments induced large patches of apoptotic cell death associated with increases in spectral slope. The combination treatments resulted in even greater apoptotic cell death. Data analysis also indicated changes in speckle histogram parameters with each treatment type. This study indicates a potential for conventional frequency ultrasound as an imaging modality possessing the capacity to non-invasively monitor response to cancer therapy in a pre-clinical SCID mouse model and the applicability of quantitative method to clinical ranges of ultrasound.

2.2 Materials and Methods

2.2.1 Experimental Design and Data Collection

Experimentation was conducted employing a SCID mouse model. Xenograft human prostate PC-3 tumors were grown on mouse hind legs for 4-5 weeks, to a size of 7-9 mm. Prior to image acquisition, mice were anesthetized with 100 mg/kg ketamine, 5 mg/kg of xylazine and 1 mg/kg of acepromazine with the tumor and surrounding area epilated (Nair™ Church & Dwight Co.). Experimentation employed 32 mice evenly divided into four treatment categories one of which remained untreated as a control group. The first

treatment set received 8 Gy in a single fraction using X-ray radiation 160 kVp X-rays given at 200 cGy/minute. The second was administered vascular targeting therapy consisting of a high concentration dose (3% v/v) of ultrasonically activated microbubbles (Definity Bristol-Myers Squibb, New York, USA) to induce vascular disruption. The last set received a combination therapy consisting of a high concentration dose (3% v/v) of ultrasonically activated microbubble anti-vascular therapy followed by an 8 Gy dose of single fraction X-ray radiation using 160 kVp X-rays administered at 200 cGy/minute. Microbubble activation was achieved via an ultrasound excitation pulse centered at 500 kHz with a pulse repetition frequency of 3 kHz and peak negative pressure of 570 kPa for a total administration time of 750ms over a 5 minute period in order to avoid any potential hyperthermic affects on the tissue [37].

Ultrasound data was collected from tumors prior to and 24 hours following treatment administration. Conventional frequency data was acquired with an Ultrasonix Sonix RP (Vancouver, Canada) system utilizing an L14-5/38 transducer operating at 7 MHz, focused at a depth of 1cm and employing a 40 MHz sampling frequency. High frequency data was acquired with a VisualSonics (Toronto, Canada) VS40b system employing a 30MHz single element f2 transducer focused at a 6mm depth and employing a 500 MHz sampling frequency. Both systems were employed to collect 3D data with scan plane distances of approximately 67 microns in the conventional frequency employing data and 15 microns in the high frequency data set. Immediately following imaging where indicated, animals were sacrificed and tumors excised for histopathologic examination. Tumor slices were acquired and stained with hematoxylin and eosin as well as TUNEL staining and light microscopy images acquired for analysis.

2.2.2 Analysis Methods

Analysis of ultrasound RF data was performed via examination of the normalized power spectrum as well as statistical analysis of the signal envelope. Ultrasound data was analyzed across 12-16 individual scan planes and consisted of conventional B-mode data in addition to raw radio-frequency (RF) signals. Analysis was performed upon a standardized region of interest (ROI) located at the tumor centre which was positioned at the pulse focal depth relative to the frequencies employed accounting for approximately 2/3 of the tumor area in cross-section size.

The power spectrum was calculated using a Fourier transform of the raw radiofrequency data individually calculated for each scan line through the ROI and subsequently averaged. In order to remove effects of system transfer functions on the employed pulses, data were normalized with a calibration pulse obtained from a flat quartz for high frequency data [44]. Conventional frequency data normalization employed the averaged power spectrum obtained from an agar embedded glass bead phantom model (modified from Madsen [45]) selected at a 1 cm focal depth as this more accurately models the frequency power distribution obtained in tissue power spectrum data than that obtained from a quartz target at low frequencies.

Linear regression analysis was performed within a 6 dB window from the peak found in the calibration pulse and a best fit line obtained. Parameters examined include the mid-band fit (MBF) which can provide acoustic backscatter and scatterer property information, the spectral slope of the best fit line within the 6 dB window which may be

related to scatterer size, and the corresponding 0-MHz intercept which may be related to scatterer concentration [38-41]. Parameters were obtained and averaged for each of the 12-16 scan planes collected per specimen and averaged for each animal and tumor for treatment category.

Statistical analysis of the signal envelope, another method to quantify ultrasound signals, employed two approaches, sample statistical and probability density function (PDF) histogram fitting analysis of statistical parameters of the envelope. Statistical analysis of the envelope was employed in order to obtain measurements of the mean, skew and kurtosis of the acquired envelope voltage distributions. Changes in the mean signal envelope intensity relative to treatment administration provided information regarding the average shift in signal amplitude correlating to overall changes in tissue echogenicity. The skewness of the data distribution provided a measurement of signal distribution relative to the mean by supplying a measurement of the symmetry of the data. Similarly, Kurtosis measurements provided a measurement of the distribution of data distant to the peak amplitude of the distribution.

In addition to statistical analysis of the signal envelope, relative differences were measured indirectly via PDF histogram fitting estimations. Envelope distributions were fitted to histograms employing an optimized bin size determined by Scott [35]. This algorithm determined optimal bin sizes relative to the standard deviation of the data, providing an independent optimal bin size for each data set. Maximal Likelihood Estimation (MLE) was subsequently utilized to fit PDF curves to the associated histograms and the resulting parameters obtained [24]. In order to assess the accuracy of determined fitted PDF curves, a Kolmogorov-Smirnov goodness of fit test was applied

[42]. PDF curves employed in this study comprised the Rayleigh, Gamma and Generalized Gamma (GG) distributions. It was found that the Rayleigh distribution provided a suitable fit to both low and high frequency data sets and was thus used in the analysis of both providing an indirect measurement of signal mean [42]. It was observed that the Generalized Gamma PDF provided an accurate representation of the distribution obtained via high frequency ultrasound data acquisition whereas the Gamma distribution was found to better match low frequency ultrasound data distributions. The two PDFs were used as the conventional frequency instrument used a different data storage range and had different sensitivity to tissue structures affecting the use of the GG PDF for the low frequency data. The GG PDF was used to calculate three parameters α , c and v . The α scale parameter represented the amplitude of the distribution at the distribution peak, while the c and v parameters indicated the proportion of the curve to the left and right of the peak respectively represented as the ratio c/v (shape parameter). The Gamma distribution parameters similarly included shape and scale parameters. Tests of significance between changes in ultrasound parameters were carried out using a T test for changes in both low-frequency and high-frequency data. A p value of <0.05 was taken to be statistically significant.

Histological analysis was carried out with tumor sections fixed in 5% formalin for 24 to 48 hours and then sectioned in 3 planes with haematoxylin and eosin (H&E) staining carried out as well as TUNEL (terminal deoxynucleotidyl transferase dUTP nick end labeling) and ISEL (*in situ* end-nick labeling) immunohistochemistry for cell death. Microscopy was carried out using a Leica DC100 microscope was used with a 20 x objective coupled to a Leica DC100 video camera wired to a 2 GHz PC running Leica

IM1000 software (Leica GmbH, Germany). Cell death areas were quantified in histology and immunohistochemistry tumor sections assisted by the use of Image-J (National Institutes of Health, Maryland, USA) macroscopically to detect ISEL positive areas in tumor sections. At higher magnifications (40X) apoptotic cells were counted manually by identifying typical apoptotic bodies.

For tumors, in order to determine cell viability, samples were excised 24 hours after treatment and kept on cold (4°C) PBS (phosphate buffered saline) to the laboratory for image processing. The skin was removed and tissue minced, and dispersed by trituration, then passed through a 70 µm sterile mesh. Cells were then washed several times with PBS, placed back into media changes and centrifuged at 800 xg between washes. The dissociated cells were then counted and serially diluted treatment at 1 x, 10 x, 100 x, and 1000 x dilutions and plated on sterile 2% agar in the presence of RPMI-1640 media and antibiotics (Sigma-Aldrich, St. Louis Missouri). Colonies were stained using methylene blue 10-14 days later and then counted manually. Only intact non-apoptotic cells were counted as being plated.

2.3 Results

Analysis of tumor responses to treatment administration was initially investigated via light microscopy image analysis employing hematoxylin and eosin, and TUNEL staining in order to quantify distinguished macroscopic regions of apoptotic tissue response. TUNEL staining for apoptotic cell death revealed an average of 1%, 6%, 11% and 60% area of apoptotic cell death within control, anti-vascular microbubble, X-ray radiation, and combination therapy treatment groups, respectively. The magnitude of response in the individual treatment categories was significantly limited when compared to the combination therapy administration indicating a potential synergistic effect of the combination therapy consistent with studies conducted by Czarnota *et al* [37]. Although tumors treated with X-rays alone did not undergo significant amounts of apoptotic cell death, high magnification analysis of hematoxylin and eosin stained tumor sections indicated that significant portions of the X-ray treated tumors demonstrated significant changes in morphology when compared to the untreated specimens with prominent mitotic arrest/catastrophe and cellular and nuclear irregularities such as cellular swelling and multi nucleated cells consistent with mitotic death [11]. Clonogenic assays of excised tumor cells from X-ray treated tumors indicated $5 \pm 2\%$ cell survival. Tumors treated with ultrasound-microbubble vascular treatment alone demonstrated central areas of apoptotic cell death. High magnification haematoxylin and eosin staining indicated the presence of apoptotic cells in clustered regions. Clonogenic assays indicated less than $30 \pm 7\%$ cell survival from these regions. Tumors treated with ultrasound-microbubble vascular disruption combined with radiation demonstrated large central patches of cell death. High magnification haematoxylin and eosin staining indicated the fulminant

presence of apoptotic cells in these large regions. Clonogenic assays indicated less than 1% cell survival from these regions.

Representative ultrasound images and data are presented in Figure 10. Ultrasound results indicated increased intensity in images with increased backscatter most obvious in the combined treatments. Mean increases in mid-band fit (MBF Δ) of 0.09 ± 0.23 dBr, 3.4 ± 0.88 dBr, 4.8 ± 0.79 dBr and 5.9 ± 0.92 dBr were observed for untreated, microbubble anti-vascular therapy, X-ray radiation, and combination therapy treatment groups, respectively. This data paralleled results observed for high frequency data yielding an observed average MBF Δ of 0.73 ± 0.83 dBr, 3.3 ± 0.58 dBr, 5.5 ± 1.32 dBr and 6.2 ± 1.15 dBr for the same treatment groups, respectively (Figure 11A). The magnitude of the increased mid-band fit correlated to an approximate 8-fold maximal increase in integrated backscatter representing significantly increased echogenicity ($p < 0.05$ for combination therapy versus untreated animals) in highly responsive tumor tissue. This morphologically correlated to changes in nuclear size in tumor specimens [14, 41]. Results obtained for spectral slope and 0-MHz intercept parameters were calculated in the same manner yielding average slope Δ and 0-MHz intercept Δ values for low and high frequency data (Figure 11 B and C respectively). Changes in slope values are displayed in Figure 11B with low frequency data yielding 0.05 ± 0.04 dBr/MHz, 0.12 ± 0.044 dBr/MHz, 0.12 ± 0.077 dBr/MHz, and 0.17 ± 0.06 dBr/MHz in the control, microbubble anti-vascular therapy, X-ray radiation and combination therapy treatment groups respectively. Results observed in high frequency data analysis yielded a similar trend of increasing slopes (-0.02 ± 0.06 dBr/MHz, 0.10 ± 0.03 dBr/MHz, 0.09 ± 0.064 dBr/MHz and 0.213 ± 0.03 dBr/MHz in the same treatment groups, respectively). These results

proved to be statistically significant with $p < 0.05$ in both high and low frequency treated data sets when compared to untreated animals, with the exception of the 8 Gy treatment set which exhibited a higher standard deviation when compared to the remaining treatment groups. Calculations of the 0-MHz intercept Δ shown in figure 11C produced a -0.27 ± 0.62 dBr, 2.87 ± 0.73 dBr, 4.07 ± 0.96 dBr, and 4.76 ± 1.23 dBr ($p < 0.005$) change in the low frequency data for the previously mentioned treatment groups, respectively. These changes trended well with results observed for the high frequency ultrasound data set which produced 0.72 ± 0.65 dBr, 1.47 ± 0.92 dBr, 3.28 ± 1.02 dBr and 4.69 ± 0.83 dBr ($p < 0.005$) changes from the pre-treatment data. The increase in 0-MHz intercept, as observed for low frequency data, was not apparent for the high frequency data for the combined treatment animals.

Statistical analysis of the signal envelope via histogram PDF fit estimations was carried out, employing the Rayleigh, Gamma, and Generalized Gamma PDFs. Statistical parameters were calculated for each independent scan line and averaged per specimen prior to and following treatment administration. The average was then computed for each treatment set and an average change computed. Figure 14 displays representative distributions prior to and following treatment which illustrate observed distribution PDF changes. Since the data storage bit resolution available in the low and high frequency data sets affected the distribution and ultimately the Rayleigh σ parameter Δ , relative changes in the Rayleigh PDF were displayed as an average $\% \sigma \Delta$ (Figure 12A). This permitted direct comparison of the low and high frequency data. Changes in the Rayleigh Sigma parameter were measured as $-2.42 \pm 1.3\%$, $32.04 \pm 4.6\%$, $41.01 \pm 7.4\%$ and $42.54\% \pm 7.3\%$ in conventional frequency data in the control, microbubble anti-

vascular therapy, X-ray radiation and combination therapy sets respectively. This data followed well with high frequency observations of $4.0 \pm 5.6\%$, $43.9 \pm 8.3\%$, $53.0 \pm 12.2\%$ and $69.7 \pm 13.06\%$ in the same treatment categories. The changes for the combined treatments were less apparent for the high frequency data.

Due to an increased data range in low frequency data, the Gamma distribution was employed whereas its special case, the generalized Gamma, was used for high frequency data. Low frequency results are shown in Figure 13 A&B. Results of the Gamma scale parameter resulted in a -3.0 ± 1.2 , 12.4 ± 2.2 , 20.1 ± 3.22 and 26.7 ± 5.51 ($p < 0.005$) observed change in the control, microbubble anti-vascular therapy, X-ray radiation and combination therapy groups, respectively. Changes in the Gamma shape parameter (Figure 13A) were observed as -0.04 ± 0.04 , -0.18 ± 0.057 , -0.49 ± 0.12 and $-0.38.28 \pm 0.11$ ($p < 0.005$) in the same treatment groups. The decrease in the shape parameter signified an increasing homogeneousness of the data as it represents a decrease in the width of the distribution near the peak, however examination of these parameters needs to be done in concert with one another as they do not act independently upon the distribution.

High frequency data employed the Generalized Gamma PDF the results of which are displayed in Figure 13 C&D. The Generalized Gamma PDF estimations provided a scale parameter α , and a shape parameter c/v . Changes in the $\alpha\Delta$ parameter were -0.04 ± 0.02 , 0.4 ± 0.1 , 0.6 ± 0.1 and 0.9 ± 0.2 in the control, microbubble anti-vascular therapy, X-ray radiation and combination therapy groups respectively. Relative changes in the c/v ratio were 0.02 ± 0.03 , 0.08 ± 0.03 , 0.08 ± 0.03 and 0.11 ± 0.03 in the same treatment groups respectively.

Calculations of the percentage change in overall signal mean are displayed in figure 12B. Low frequency data analysis observed changes of $-3.03 \pm 1.3\%$, $40.2 \pm 12.3\%$, $49.1 \pm 14.3\%$ and $57.58 \pm 13.9\%$ ($p < 0.005$) in the control, microbubble anti-vascular therapy, X-ray radiation and combination therapy treatment groups, respectively. Results in the HFU range were measured as $6.5 \pm 5.5\%$, $45.7 \pm 10.0\%$, and $56.5 \pm 16.5\%$ and $69.8 \pm 14.0\%$ ($p < 0.005$) in the same treatment sets. Measurements of skew were $7.7 \pm 6.5\%$, $27.5 \pm 9.48\%$, $56.4 \pm 15.9\%$ and $70.9 \pm 18.4\%$ ($p < 0.001$) in the respective treatment groups. High frequency analysis saw a $2.9 \pm 2.1\%$, $7.8 \pm 2.6\%$, $28.9 \pm 5.6\%$ and $5.5 \pm 2.2\%$ in the same data sets respectively. Examination of these results with observed measurement in the PDF estimations substantiate findings that low frequency data undergoes a much larger change in symmetry about the signal mean when compared to results observed in the high frequency analysis. In order to gauge the portion of the data located at ends of the distribution, measurements of kurtosis were undertaken and are shown in Figure 12D. Changes in Kurtosis values observed in the LFU data were measured to be $3.7 \pm 4.1\%$, $21.5 \pm 5.6\%$, $46.5 \pm 12.3\%$ and $58.0\% \pm 11.9\%$ in the respective treatment categories. Measurements of changes in Kurtosis within the HFU data set resulted in 2.35 ± 1.7 , 6.42 ± 1.88 , $20.35 \pm 4.08\%$ and $8.78 \pm 3.74\%$ in the same treatment sets.

2.4 Discussion

The results demonstrate for the first time that low-frequency ultrasound may be used to detect cell death *in vivo* in well controlled preclinical animal models of cell death. Compared to untreated control animals both spectroscopic ultrasound analyses (analyzing mid-band fit, spectral slope and 0-MHz intercept parameters) and speckle statistics (scale and shape parameters from Gamma and Generalized gamma probability distribution functions) indicated consistent changes associated with increases in cell death. Different forms of cell death were detectable in response to predominantly mitotic death induced by 8 Gy radiation treatments, apoptosis induced by anti-vascular death secondary to ischemia and greater amounts of apoptotic death in the combination treatments.

Changes in B-mode images with different treatments were visually apparent as presented in Figure 10. Samples which displayed histologically prominent macroscopic areas of cell death demonstrated increased backscatter in the low and high-frequency ultrasound images. Increases in backscatter ranged from 1 to 6 dB for samples concordant with increase in cell death apparent histologically.

Spectral data indicated coincident increases between the ultrasound ranges in terms of mid-band fit and slope. Observed increases in slope with the different treatment types are consistent with the interpretation of scatterer sizes becoming smaller. For instance, it has been previously demonstrated that nuclear morphology influences scatter mid-band fit and slope in both the high and low-frequency ranges in which condensed and fragmented nuclear material from normal and apoptotic cells and their isolated nuclei were able to cause increases in ultrasound backscatter from 10 to 50 MHz consistent with that for cells

alone [24]. In this thesis, increases in the 0-MHz intercept, which can be related to the concentration of acoustic scatters also occurred with the exception of the combined treatment set in which this was less apparent with high-frequency ultrasound. We suspect that the nuclear degeneration and disintegration which was most prominent in this sample has a greater effect upon high-frequency data, with a near complete loss of cell structure leading to a decrease in this parameter.

Changes in speckle statistics were also apparent with cell death. This measure has been used before with cells treated with chemotherapy [10, 33]. These results indicated concordant shifts in scale parameters for low-frequency and high-frequency data but slightly different changes in shape parameters. This may be attributed to the differences in scales of change between the treated data sets with low frequency data exhibiting a substantially larger increase in scale than that observed in the high frequency data.

This data in this study is supported by previous investigations of cell death detection using high-frequency data in which models *in vitro* and *in vivo* have been analyzed. These include cells and normal tissues rendered apoptotic using a variety of modalities. That work indicated an important role in nuclear structure in the detection of cell death. Changes which induced nuclear condensation either by the induction of mitotic death or apoptotic death lead to increases in backscatter. That was borne out in this study in high and low-frequency data. Other work comparing low-frequency and high-frequency data predominantly from *in vitro* cell models indicated a correspondence such as that seen here for experiments done following cell death progression with time and cell death concentrations. Samples which were imaged here which showed increases in cell death

had consequent changes in spectral and statistical parameters which mirrored the trends in histologically detected cell death.

The fact the low-frequency data were mirrored in trend by the high-frequency data was also reassuring although the type of scatter expected from the two samples is different. We would expect Mie-type scattering with high-frequency ultrasound whereas at low-frequency we would expect Rayleigh scattering to predominate. That both ranges of ultrasound are sensitive to cell death are not necessarily surprising. We have recently demonstrated the use of low-frequency ultrasound to detect cell death *in vitro* with AML cells [25]. We have also demonstrated that the condensation of nuclear material can induce increases in backscatter in the low-frequency range using isolated nuclei from viable and apoptotic cells. Moreover, the results are consistent with long-standing observations that tissue responses to therapy could be detected using ultrasound [8].

In conclusion this study indicates for the first time that quantitative low-frequency ultrasound may be used to detect cell death *in vivo* and is supported by corresponding high-frequency ultrasound data. Data were obtained for three different manners of inducing cell death in preclinical prostate cancer xenografts and analyses indicated concordance between ultrasound changes and the histopathological extent of cell death. This work forms the basis for the application of such low-frequency approaches *in vivo* in cancer patients for the monitoring and customization of their cancer therapies.

Chapter 3 - Conclusion and Future Work

The aim of this study was to assess the efficacy of conventional frequency ultrasound as a means of detecting structural changes in tumor tissue in response to cancer therapy. It was demonstrated in this thesis that ultrasound employed at a clinically relevant frequency does exhibit significant changes in backscatter characteristics as a result of tumor therapy administration. This was assessed via experimentation involving PC-3 tumors grown on SCID mice treated with a variety of cancer therapies. Examination of the power spectrum obtained from tumors before and after treatment administration indicates a maximal 8-fold increase in tissue echogenicity accompanied with changes in power spectral parameters. Observed changes in spectral slope and 0-MHz intercept were consistent with theoretical models correlating to scatterer size and concentration. The increase in spectral slope is consistent with theoretical predictions of scattering from smaller structures and increases in 0-MHz intercept consistent with theoretical predictions of increases in scatterer concentration. Additionally, statistical analysis of the signal envelope demonstrated significant changes in the distribution obtained from tissue prior to and following treatment administration. These changes included parameters obtained through PDF curve estimations as well as measurable changes in signal mean and symmetry.

Although this study does provide a starting point as a proof of principle examination, there is work required before this research can be utilized. Future experimentation employing time course studies will provide an indication of the potential of low frequency ultrasound as a method of early assessment of patient response. Although this

study did observe changes in response to treatment, it is lacking in that examination of parameters was conducted at a single time after treatment. It has been shown through previous study that tumors exhibit maximal apoptotic response 24 hours following treatment administration [25, 37]. This made the selection of this time point suitable for initial examination as corroborated through histological examination of treated tumors. Work *in vitro* employing clinically relevant ultrasound frequencies has demonstrated detectable changes in spectral parameters as early as 6 hours following treatment administration [25]. Examination within further *in vivo* models would allow for the further assessment of low frequency ultrasound as an early indicator of treatment effectiveness. A wider range of tumor cell lines and therapy combinations would demonstrate the robustness of the method. This will permit the assessment of low frequency ultrasound in detecting changes in tumors possessing a variety of morphological characteristics as well as exhibiting different therapeutic responses. The induction of various modes of cell death should be examined as it has been shown in *in vivo* models that they present significantly different changes in spectral parameters. This is something which was observed in this thesis in which tumors possessing various concurrent modes of cell death were examined. The induction and observation of various modes of cell death in an *in vivo* model may allow for a more accurate assessment of treatment response in a clinical setting.

The examination of tumor response provides invaluable information regarding treatment response however the presentation of this information is critical for use in a clinical setting. As such a preliminary parametric imaging technique was designed to visually represent changes in spectral parameters. The generation of an imaging modality capable

of visually presenting structural changes in tissue would aid clinicians in assessing patient response by providing information regarding response magnitude and distribution. This approach has been applied in a wide variety of medical applications allowing for information to be conveyed in a user friendly and direct manner.

A preliminary parametric imaging modality has been implemented in order to gauge the potential of representing analytical results in a clinically effective manner. Parameters obtained via power spectrum analysis have been incorporated into a parametric mapping scheme providing color coding of analysis regions. This technique was initially investigated employing a region segmenting algorithm which evenly divided the analysis region into quadrants in which spectroscopic analysis was conducted. Each pixel within individual quadrants was then assigned values based upon the resulting calculated segment parameters. As displayed in Figure 15, this method does visually convey information regarding relative changes backscatter intensities, however this information is lacking in depth. As every pixel within a quadrant is identically assigned, there is a significant loss in image resolution.

In order to increase parametric resolution, the technique has been enhanced through implementation of a sliding window algorithm. This employs a fixed size window of surrounding data in which parameters are calculated for each image pixel and subsequently shifted for each. Although this significantly increases processing requirements by increasing the amount of data processed during image generation, the resulting parametric overlay contains information regarding the distribution of the parameters throughout a calculated ROI. The sliding window algorithm calculates the power spectrum for each individual scan line in the window then determines an average

across the section. The averaged power spectrum is then normalized with a reference pulse and linear regression parameters computed within a -6 dB window. This is repeated for each individual pixel resulting in a color map of the analysis region based upon individual analysis parameters.

Figure 15 displays the results of parametric images calculated for the mid-band fit spectral parameter employing both the segmented and sliding window algorithms. Reconstructed B-mode images display two centrifuged cell samples and selected analysis regions. One sample (right) contains untreated AML cells and the other (left) an AML cell sample exposed to the chemotherapeutic agent cisplatin for a period of 12 hours. Although the segmented algorithm is capable of clearly distinguishing backscatter increases from the bottom of the housing well and the top of the cell pellet, it does not possess the capacity to clearly display the relative increases in backscatter obtained from treated and non-treated samples. As is evident from Figure 15, implementation of the sliding window algorithm increased parametric resolution. The algorithm is capable of clearly delineating the well and pellet surfaces and most significantly displays differences in echogenicity between the treated and untreated samples. Figure 16 displays B-mode images containing parametric overlays of calculated regions of interest of PC-3 tumor xenotransplants prior to and at 24 hours following various treatments examined in this study. These images are calculated for the mid-band fit parameter and provide a visual representation of increased backscatter in response to treatment administration examined in this study.

The parametric technique does provide a positive indication that an imaging algorithm can be developed in order to visually represent analytical data, however it is not

sufficiently sophisticated in its representation in that it currently only accounts for a single calculated parameter. Further investigation into the development of this technique should begin with the examination of a method incorporating a variety of analysis parameters. This will require investigation into various weighting algorithms and parameter combinations. The use of multi-parameter image generation should examine various combinations of windowing and segmenting techniques. For example it may be found that statistical data may contribute regional information thus employing a region segmenting approach in combination with spectral parameters obtained via a sliding window approach. Additionally there is potential in the use of machine learning techniques such as neural network perceptrons which have been demonstrated to be effective when attempted in other tissue classification applications [17, 43].

In conclusion, the work presented in this thesis provides a proof of principle examination into the efficacy of ultrasound employed at 7 MHz to detect changes in cancer tissue as a response to treatment. The examination of various treatment administrations and responses provides a positive indication that low frequency ultrasound may be one day employed as a method of non-invasively assessing patient response to cancer therapy in a clinical setting. In order for this to become a reality, there is a need for a significant amount of research in the characteristics of ultrasound across frequencies and treatment scenarios as well as the generation of an algorithm encompassing multiple parameters to represent these characteristics in a useful manner. This presents a large body of work, however the potential benefits of this research may one day have an enormous impact on patient care by allowing clinicians to assess patient response to therapy at early stages.

Appendix

A.1 Experimental Design

This study was conducted via *in vivo* experiments employing 32 severe combined immunodeficient (SCID) mice. Human prostate PC-3 cells were employed to grow tumors as xenotransplants on the hind legs of mice. Tumors were grown for a 4-5 week period growing to an average longitudinal length of approximately 8-10 mm at which point they were treated with vascular damaging microbubbles, 8 Gy X-ray radiation and combinations of these therapies.

A.2 Data Collection

Once tumors were grown sufficient for experimentation data collection was initiated. Mice were anesthetized with 100 mg/kg ketamine, 5 mg/kg of xylazine and 1 mg/kg of acepromazine with the tumor and surrounding area epilated with Nair™ (Church & Dwight Co.). In order to acquire ultrasound data, mice were restrained with tape to reduce potential movement and the hind leg tumor placed in a bath of degassed water. Ultrasound gel was employed to seal the bath as well as cover the tumor for ultrasound data acquisition.

Conventional frequency data was collected with an Ultrasonix RP system employing a 128 element 3.8 cm L14-5 transducer operated at 7 MHz and focused at a depth of approximately 1 cm employing a sampling rate of 40 MHz. Data acquisition was accomplished in a single pass longitudinally across the tumor length. As the equipment setup employed does not allow for automated steps across the acquisition area, the transducer was attached to a slider and manually moved across the scan plane by

manipulation of a knob controlling the sliding mechanism. As the movement rate was maintained consistently throughout the acquisition, an estimation of distance between data frames could be calculated. The average number of acquired frames for each tumor was approximately 150 across tumors averaging 10mm in length, resulting in an average frame separation distance of approximately 67 microns. As such, the data analysis was conducted on frames separated by an average of seven frames. High frequency data was collected using a VisualSonics VS40b system with access to raw radiofrequency data. Data was collected employing a 30 MHz single element f2 transducer pulsed at 25MHz focused at a depth of 6 mm employing a sampling rate of 500 MHz. The transducer was attached to a mechanical arm allowing for controlled steps across the tumor length. High frequency data was collected across 30 steps for each tumor, with each radiofrequency scan line collected over five passes as seen in Figure 9.

A.3 Data Analysis

Data analysis was performed using a customized software package (RAWAnalyzer) developed during this thesis in the MATLAB environment. This software was used to analyze radiofrequency data acquired from both imaging devices employed in this study. The RAWAnalyzer was used to perform analyses of power spectra as well as statistical analysis of signal envelope using data from a user defined region of interest.

As depicted in Figure 9, region of interest selection was conducted employing different selection criteria in the two frequencies employed. As high frequency ultrasound can be considerably affected by attenuation effects when propagating through tissue (discussed in section 1.3), it does not typically possess a considerable tissue penetration depth.

These regions of interest were selected near the tumor where the transducer was focused and did not encompass a large area of the tumor surface when compared to conventional frequency analysis. Analysis regions selected in the conventional frequency data was centered at the transducer focus at a depth of 1cm with windows encompassing approximately two thirds of the tumor area in cross section, while analysis regions selected for the high frequency files were centered at a 6mm focal depth and encompassed a smaller area of the tumor tissue.

A.4 L14-5/38 Transducer Characterization

Prior to data analysis, an investigation into the characteristics of the 3.8 cm L14-5 transducer employed in the conventional frequency data collection was conducted. This investigation was necessary in the selection of an appropriate linear regression analysis bandwidth and in the confirmation of data acquisition quality from tumor data acquisition. As there has been considerable research conducted employing the single element 30MHz f2 transducer for high frequency *in vivo* experimentation, the characterization of that transducer has been previously been investigated by [22,33].

Analysis of spectroscopic data employed a -6 dB bandwidth employing power spectra obtained from an agar embedded glass bead phantom which was selected as its backscatter better mimics that of tissue. The -6 dB bandwidth was selected as it contains 50% of the power within the spectra, and is widely employed in the literature. In order to confirm that this window contains a sufficient signal to noise ratio for data analysis, the spectra obtained from backscatter acquired from degassed and distilled water in addition to that acquired from an agar embedded glass bead phantom was analyzed and are shown

in Figure 5. The corresponding power spectrum indicates that the majority of the power spectra signal approximately within the 2-8 MHz frequency range. As the bandwidth corresponding to the glass bead phantom reference peak was approximately 4-7.5MHz, this implies that this window was sufficient for analysis in keeping with other analysis of power spectra.

Comparison of the signal amplitude obtained from the phantom reference and water spectra provided an indication of the signal to noise ratio. As the backscatter through the water medium should produce no backscatter, the spectra obtained from this acquisition indicate the amount of noise in the system during acquisition. The spectra obtained from the phantom reference should be primarily based upon the backscatter signal with a sufficient signal to noise ratio. The peak amplitude observed in the water acquisition spectra was approximately 50 dB. When compared to the approximately 95dB peak obtained in the phantom backscatter spectra it was found that there was a sign sufficient ratio of signal to background noise.

In order to confirm that the data acquisition was consistent across frequency ranges, the spectra obtained from both data sets was compared (Figure 6). The normalized power spectra encompassing analysis frequencies of the high and low frequency data sets were fit upon a single graph in order to investigate any potential discrepancies in data collection or normalization across the frequency ranges. The normalized power spectra were obtained from a single tumor treated with a combination therapy of vascular targeting microbubble and X-ray radiation treatments. The resulting graph does not indicate any substantial divergence in spectral amplitude levels nor show considerable variation in the slope of the calculated linear regression line.

Figures

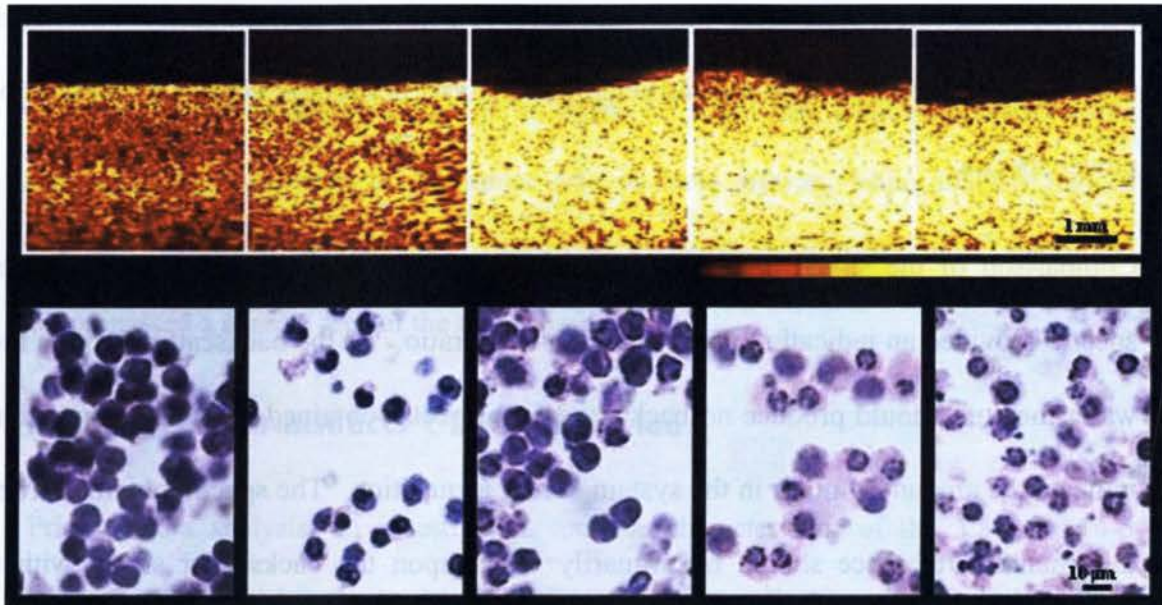


Figure 1: High frequency ultrasound images of acute myeloid leukemia cells and corresponding TUNEL stained light microscopy images. Acute myeloid leukemia cells have been exposed to the chemotherapeutic agent cisplatin for 0, 6, 12, 24 and 48 hours (left to right panel, respectively). The increase in cell echogenicity correlates with maximal apoptotic response at 24 hours. Lookup table colour bar corresponds to pixel values of 0 on the left and the right the color corresponding to a pixel value of 256. Image reproduced from Czarnota *et al.* [9]

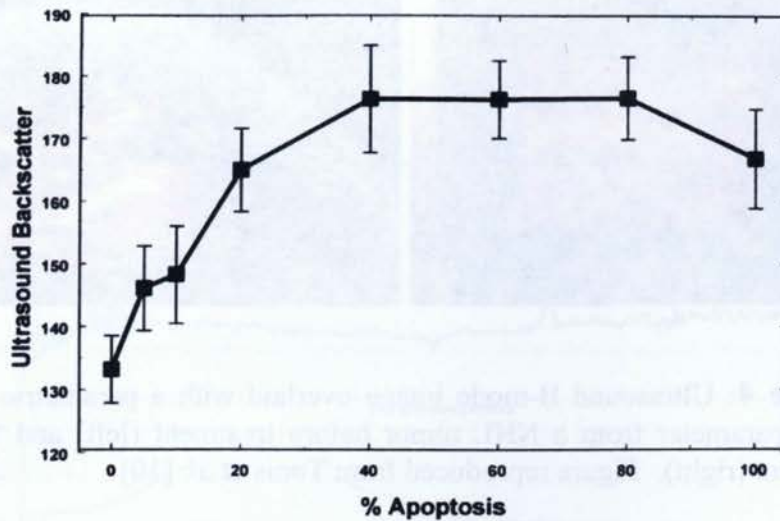


Figure 2: Backscatter intensity measurements of acute myeloid leukemia cell populations with varying concentrations of apoptotic cells. Increases in backscatter amplitude measurements correlate with increasing apoptotic elements peaking at a 40% - 80% concentration within the population. Figure reproduced from Czarnota *et al.* [9]

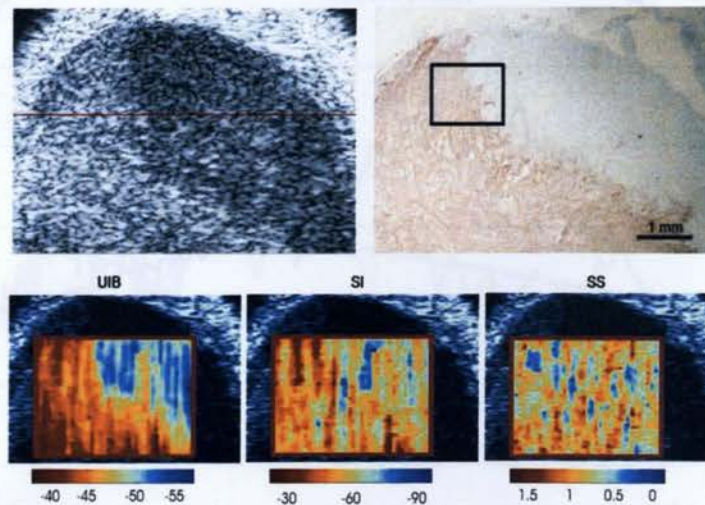


Figure 3: Ultrasound image of human head and neck tumor with corresponding histology and parametric images. Top left shows an ultrasound B-mode image and right corresponding TUNEL-stained image indicating an area of cell death of similar shape as the hyper-echoic area in the ultrasound image and parametric images computed from the local estimates of ultrasound integrated backscatter (UIB), spectral intercept (SI), and spectral slope (SS). The color-bars under each parametric image indicate the ranges of the corresponding estimates of the spectral parameters. Figure reproduced from Vlad *et al.* [11]

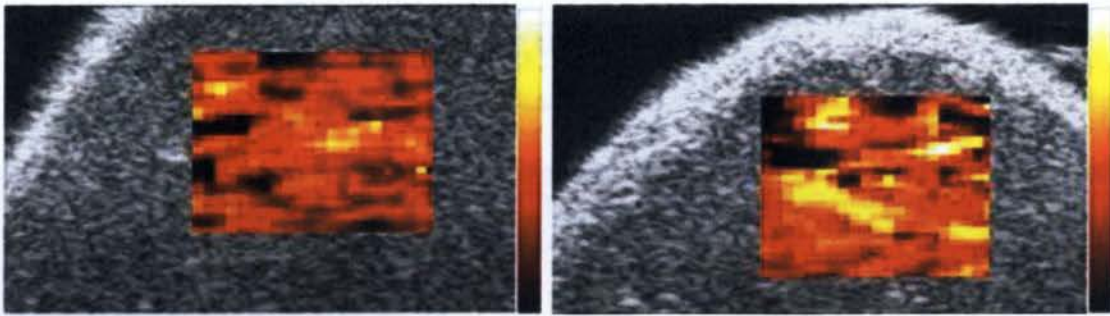


Figure 4: Ultrasound B-mode image overlaid with a parametric image of the GG α parameter from a NHL tumor before treatment (left) and 12 hours post treatment (right). Figure reproduced from Tunis *et al.* [10]

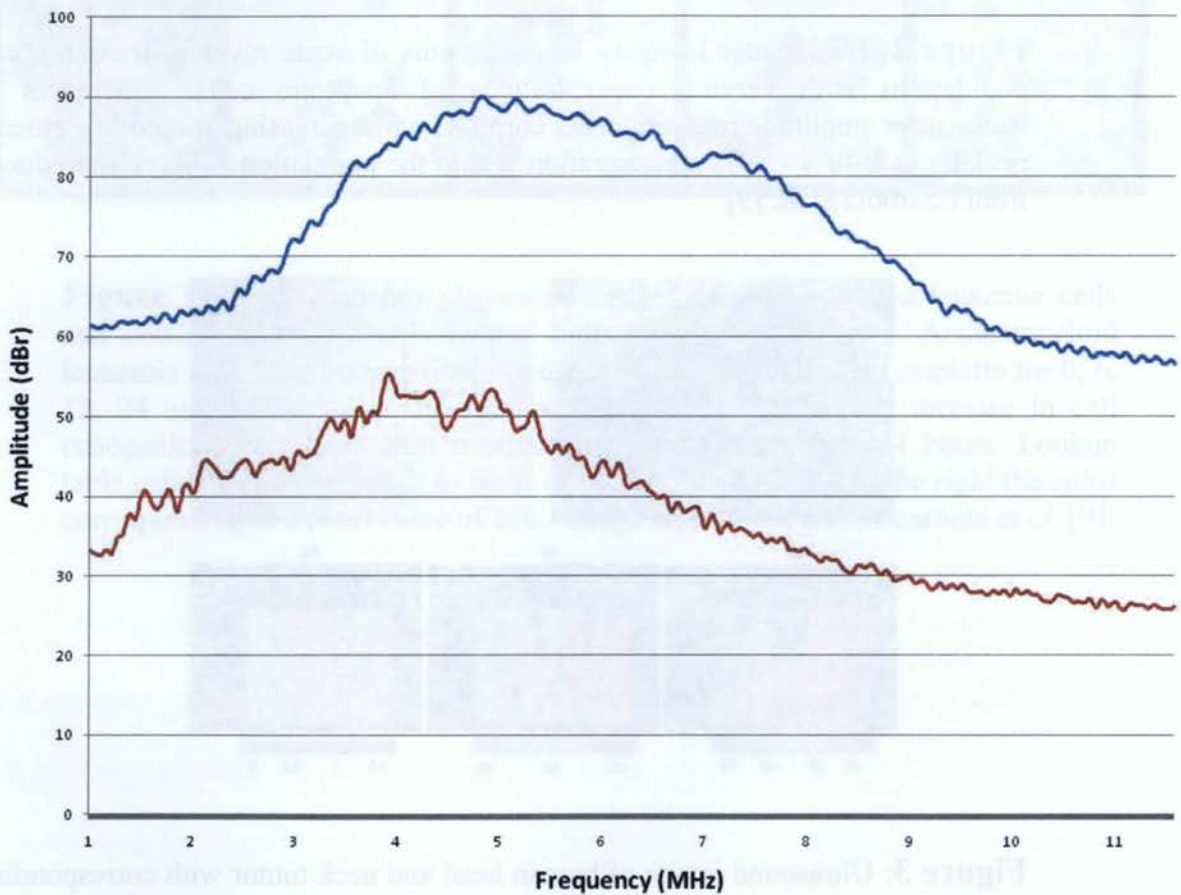


Figure 5: Power spectra obtained from water indicating the system noise detected by the employed transducer (bottom) and from an agar embedded glass bead phantom (top).

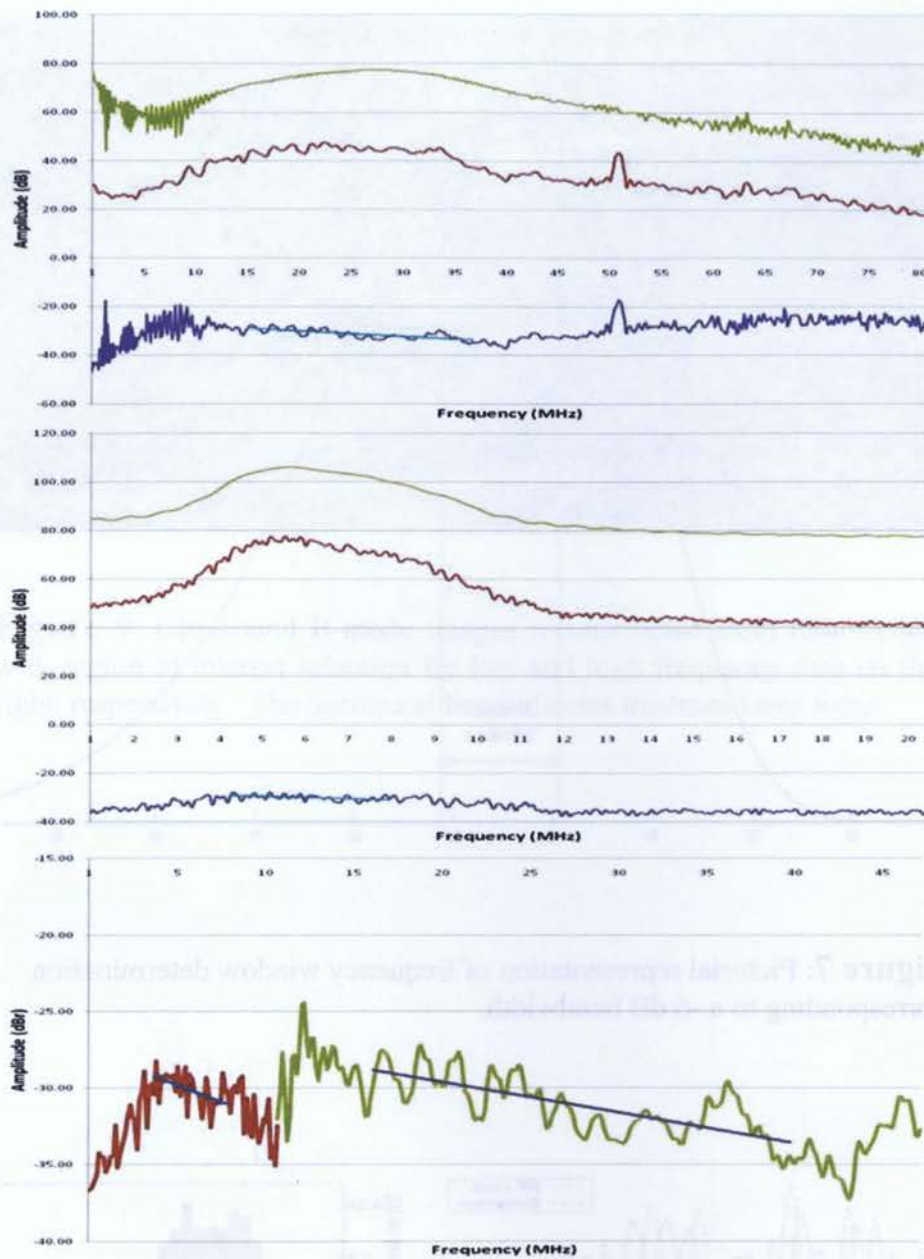


Figure 6: Representative normalized power spectra obtained using high frequency ultrasound from PC3 tumor administered microbubble anti-vascular therapy followed by 8 Gy X-ray radiation treatment (top). Power spectra shown from the reference pulse, region of interest, and corresponding normalized spectra with best fit line from top to bottom, respectively. Representative normalized power spectra obtained using low frequency ultrasound from PC3 tumor administered microbubble anti-vascular therapy followed by 8 Gy X-ray radiation treatments (middle). Power spectra shown from the reference pulse, region of interest and corresponding normalized spectra with best fit line, from top to bottom, respectively. Normalized power spectra from low and high frequency data and corresponding best fit line within a 6 dB window (bottom).

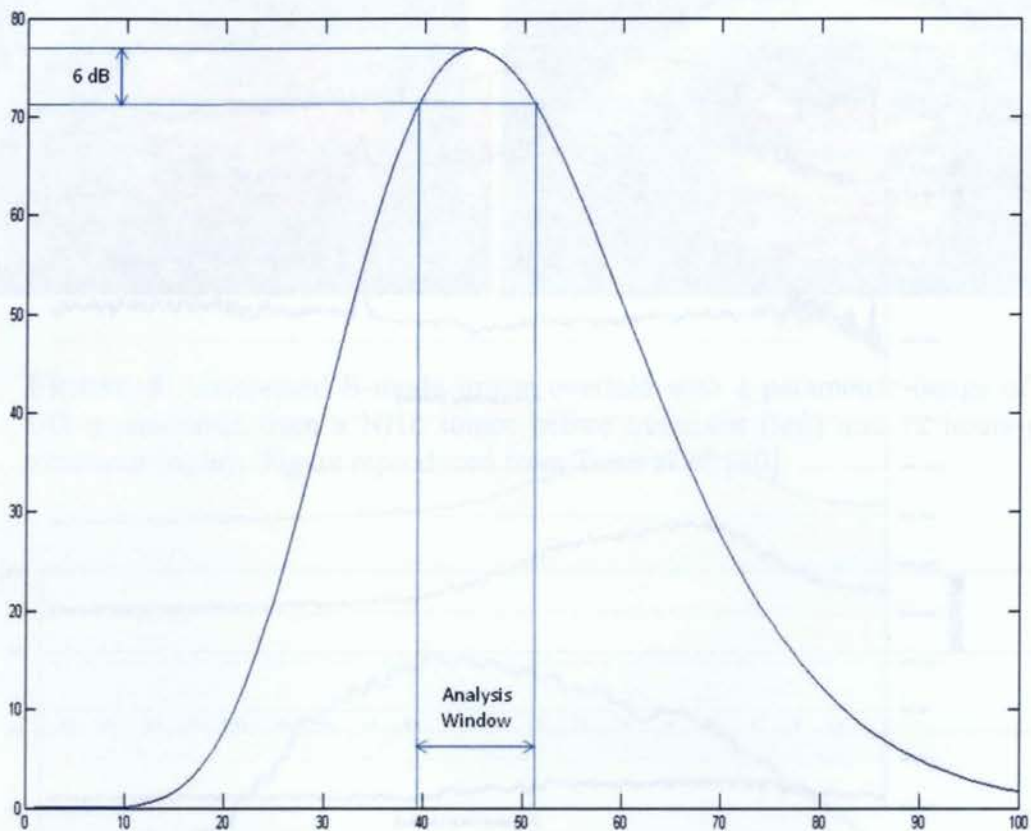


Figure 7: Pictorial representation of frequency window determination corresponding to a -6 dB bandwidth.

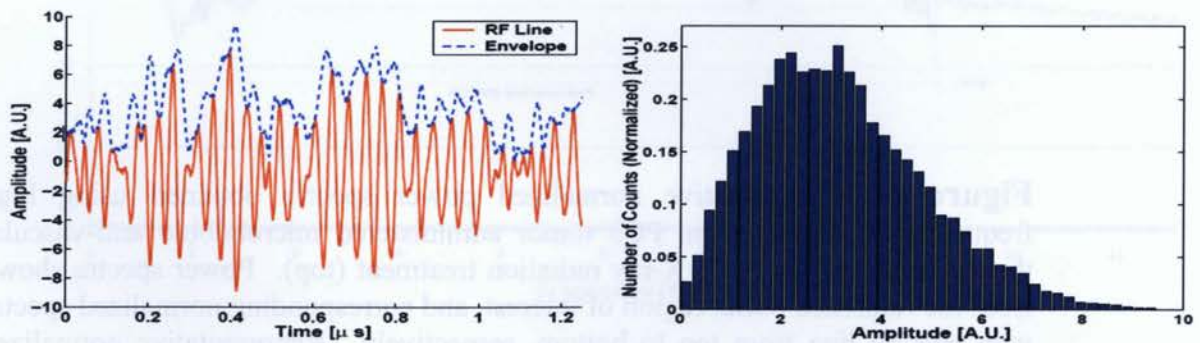


Figure 8: A sample radiofrequency line, with its corresponding envelope, and the histogram of the envelope amplitude, normalized to an area of one. Reproduced from Tunis *et al* [33].

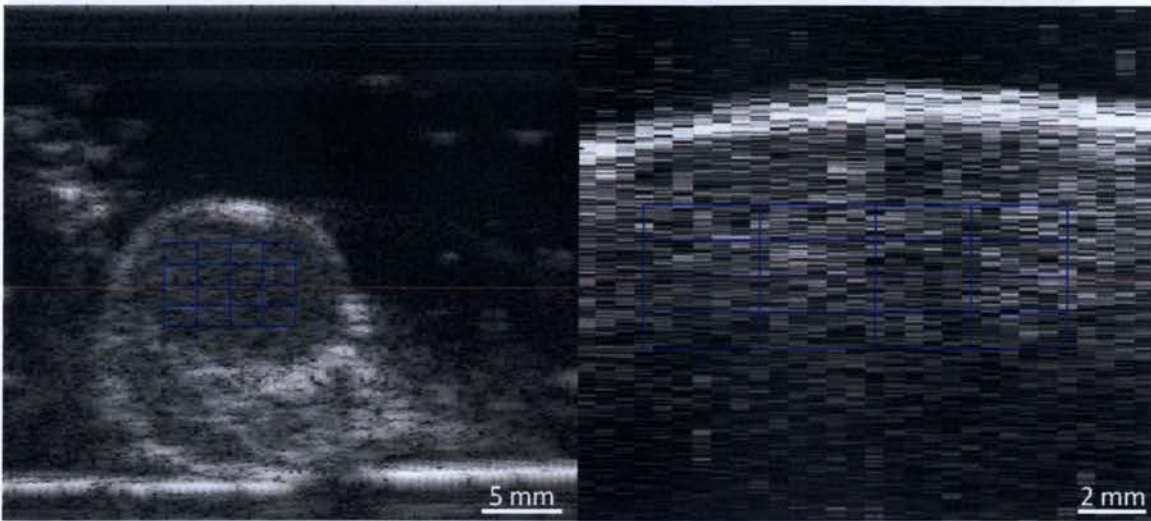


Figure 9: Ultrasound B-mode images reconstructed from radiofrequency data with region of interest selection for low and high frequency data on the left and right, respectively. The horizontal line indicates the transducer focus.

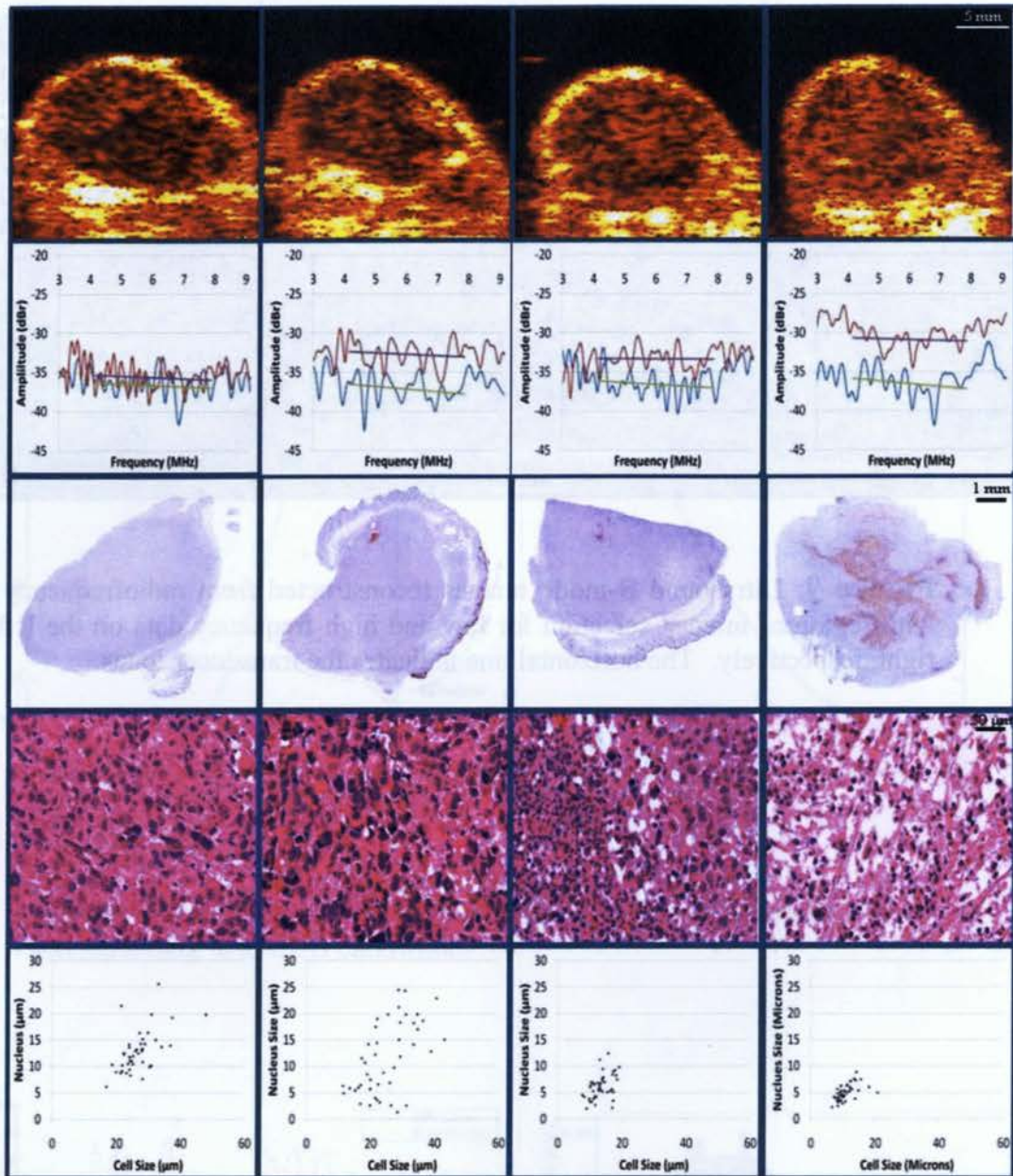


Figure 10: Representative data from untreated, 8 Gy X-ray, anti-vascular microbubble and anti-vascular microbubble followed by 8 Gy X-ray treatment administration groups, from left to right, respectively. Representative 7 MHz ultrasound B-mode images of PC3 tumors demonstrating increases in tissue echogenicity with treatment administration in contrast to untreated tumor (first row). Representative normalized power spectra obtained from PC3 tumors prior to treatment and at 24 hours following treatment administration (second row). Low magnification light microscopy images of TUNEL stained PC3 tumors (third row). Light microscopy images of H&E stained tumor slices obtained at high magnification (fourth row). Distribution of cell versus nucleus size measurements representing morphology of responsive regions within the tumor (fifth row).

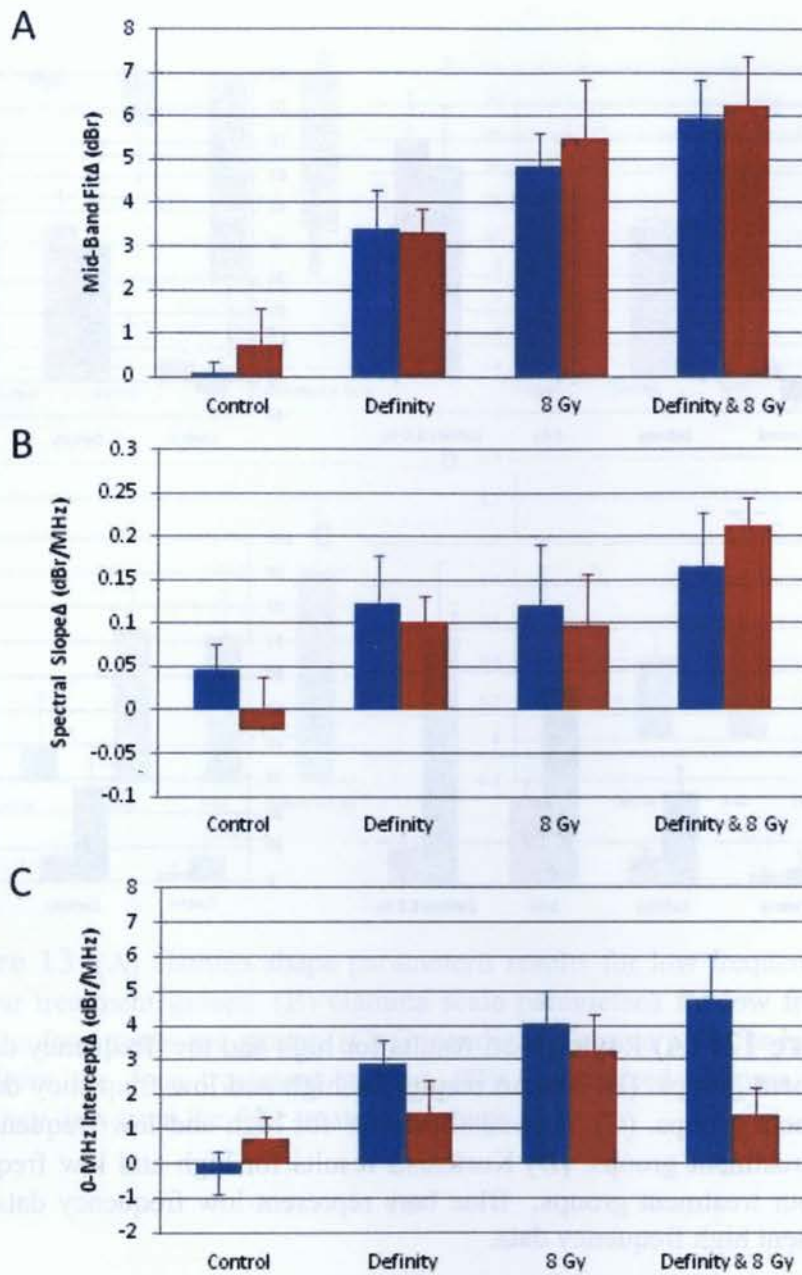


Figure 11: (A) Mid-band fit Δ results for high and low frequency data in the four treatment groups. (B) Spectral slope Δ results for high and low frequency data in the four treatment groups. (C) Zero-MHz intercept Δ results for high and low frequency data in the four treatment groups. Blue bars represent low frequency data and red bars represent high frequency data.

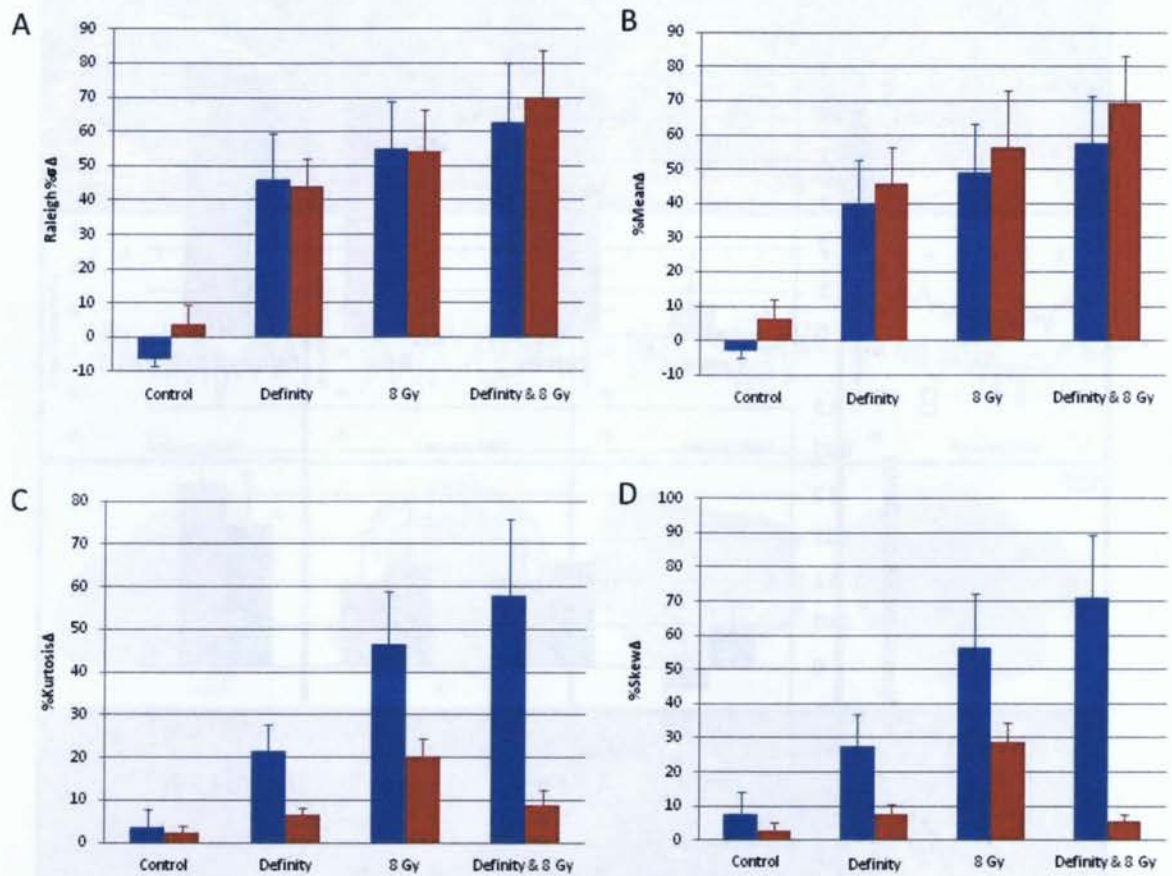


Figure 12: (A) Rayleigh $\sigma\Delta$ results for high and low frequency data in the four treatment groups. (B) Mean Δ results for high and low frequency data in the four treatment groups. (C) Skewness Δ results for high and low frequency data in the four treatment groups. (D) Kurtosis Δ results for high and low frequency data in the four treatment groups. Blue bars represent low frequency data and red bars represent high frequency data.

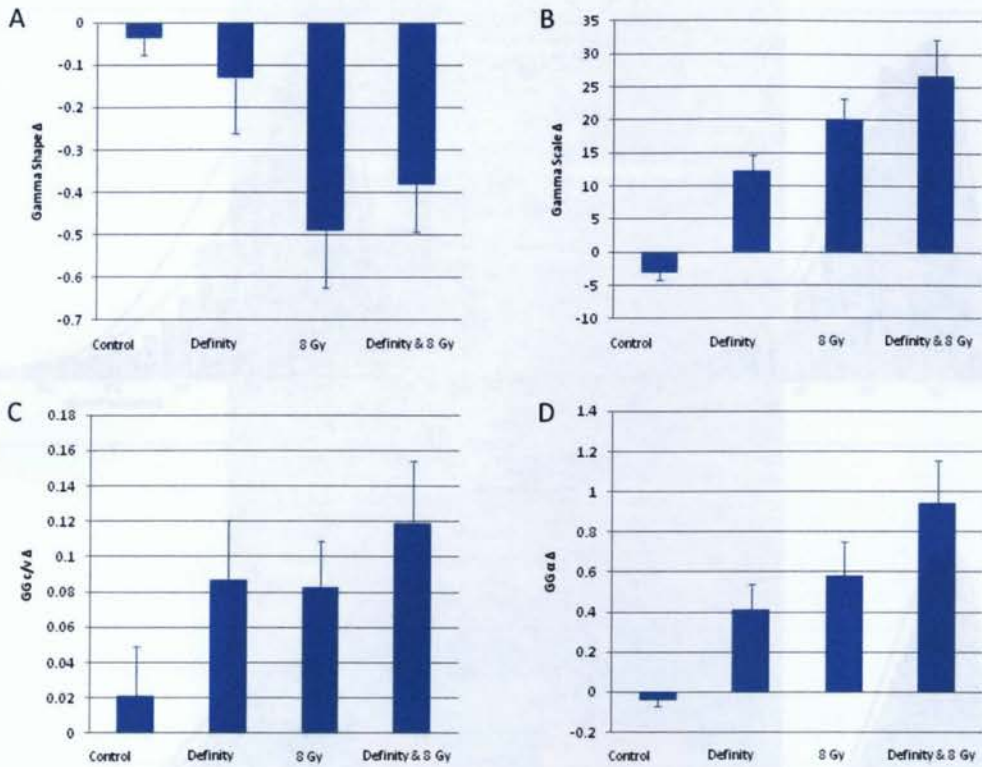


Figure 13: (A) Gamma shape parameter Δ results for low frequency data from the four treatment groups. (B) Gamma scale parameter Δ for low frequency data from the four treatment groups. (C) Generalized Gamma $c/v\Delta$ for high frequency data from the four treatment groups. (D) Generalized Gamma $\alpha\Delta$ for high frequency data from the four treatment groups.

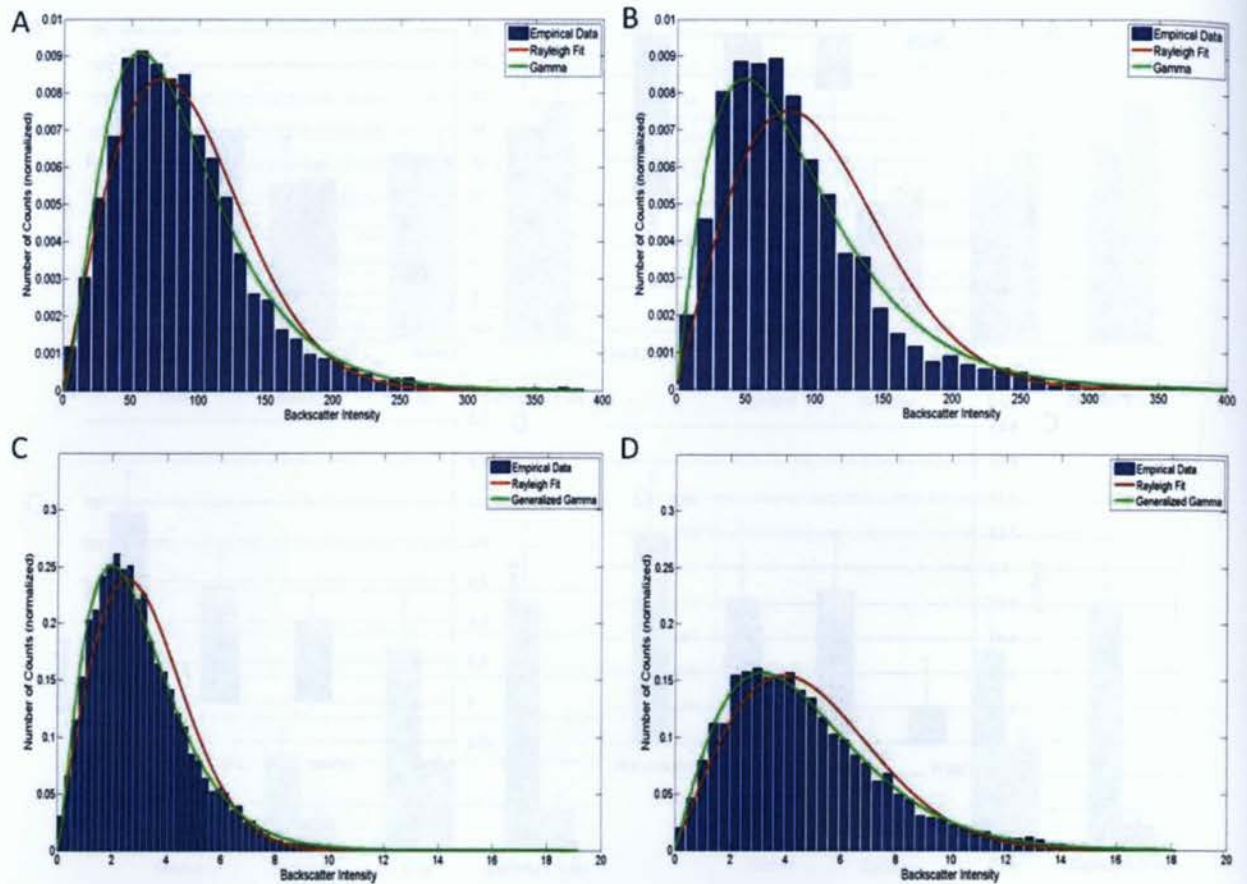


Figure 14: Low frequency ultrasound signal envelope amplitude distribution histogram with Rayleigh and Gamma PDF estimations from untreated and microbubble followed by X-ray radiation treated PC3 tumor (A and B, respectively). High frequency ultrasound signal envelope amplitude distribution histogram with Rayleigh and Generalized Gamma PDF estimations from untreated and microbubble followed by X-ray radiation treated PC3 tumor (C and D, respectively).

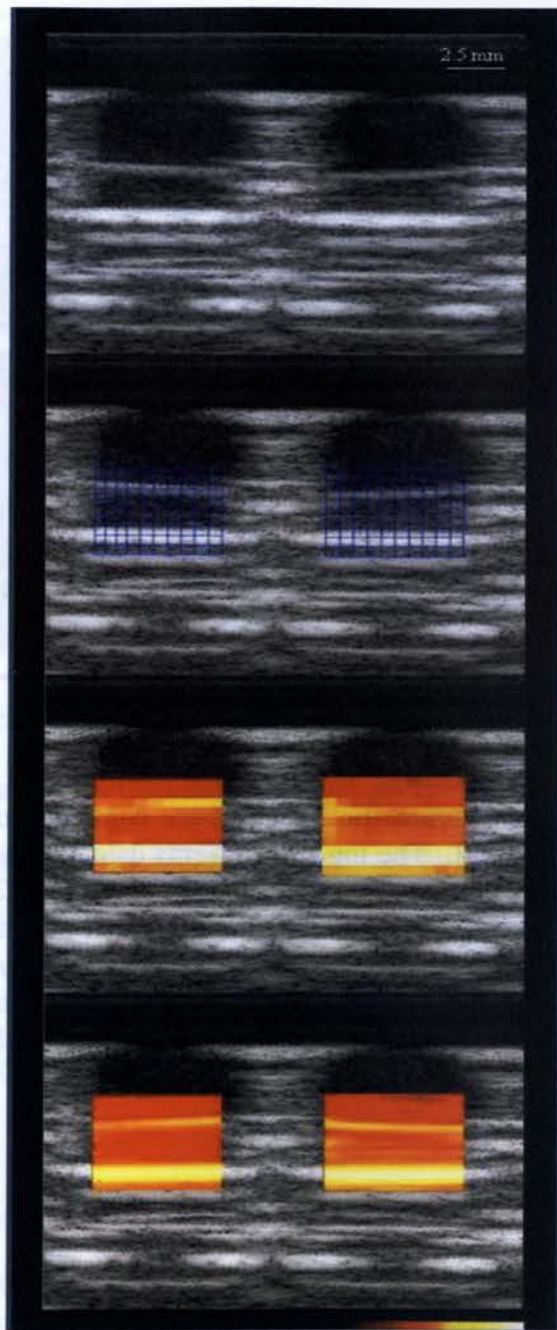


Figure 15: Low frequency ultrasound B-mode images of sample wells containing acute myeloid leukemia cells (top) and region of interest selection (second from top). The left well contains untreated cells and the right well contains cells exposed to the chemotherapeutic agent cisplatin for a 12 hour period. The third image from the top displays parametric image overlays employing a region segmentation algorithm. The bottom image displays parametric image overlays employing a sliding window algorithm. Parametric scale bar corresponds to mid-band fit values of of -100 dBr on the left and 0 dBr on the right.

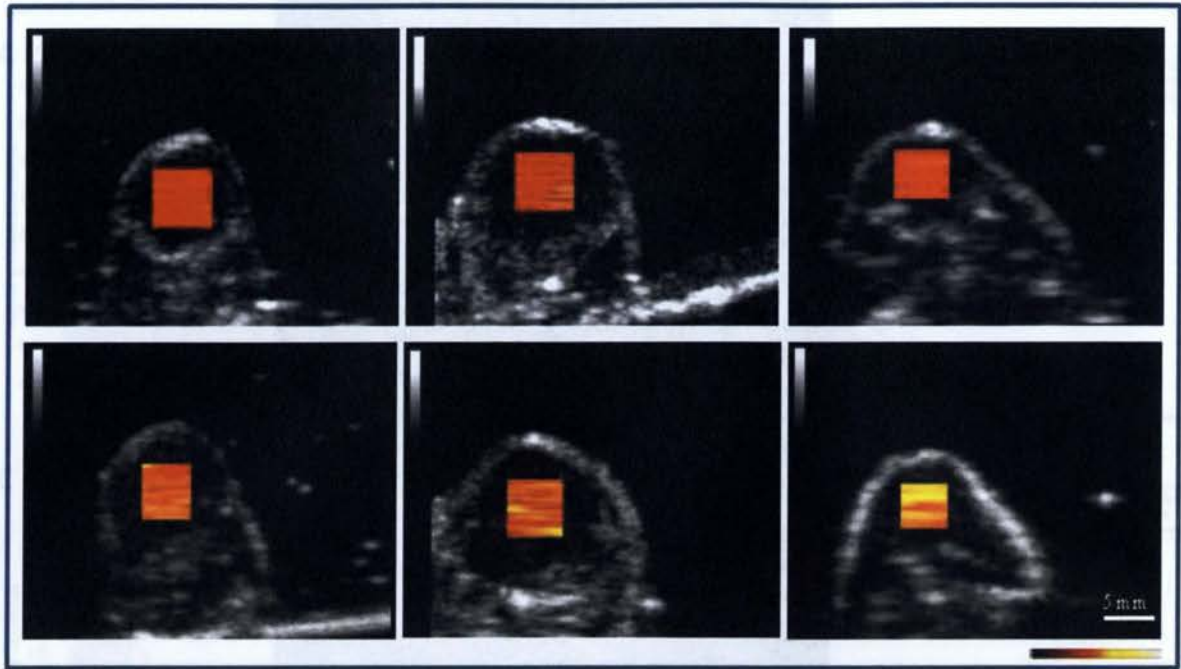


Figure 16: Representative low frequency ultrasound B-mode images with parametric overlay. Parametric images were computed using a sliding window algorithm within a ROI. The top row presents data obtained from tumors prior to treatment and the bottom data collected from tumors 24 following treatment administration. Treatment administration consisted of anti-vascular microbubble alone, 8 Gy X-ray radiation and anti-vascular microbubble and 8 Gy X-ray radiation combination treatments from left to right respectively. Parametric scale bar corresponds to mid-band fit values of of -100 dBr on the left and 0 dBr on the right.

References

- [1] K Brindle, New approaches for imaging tumour responses to treatment.
Nat Rev Cancer 2008: pp 94 - 107.
- [2] F Forsberg, Ultrasonic biomedical technology; marketing versus clinical reality.
Ultrasonics 2003: 42: pp 17 - 27.
- [3] RSC Cobbold, Foundations of Biomedical Ultrasound: pp 7.1 - 7.2
- [4] JJ Faran, Sound scattering by solid cylinders and spheres.
J Acoust Soc Am 1951: 23: pp 405 - 418.
- [5] R Baddour, High frequency ultrasound scattering from microspheres and single cells.
Master's thesis, University of Toronto, ISBN 0973485019, 2004.
- [6] JA Zagzebski, Essentials of Ultrasound Physics: pp 13 - 15.
- [7] JW Strutt, Investigation of the disturbance produced by a spherical obstacle on the waves of sound.
Proceedings of the London Mathematical Society 1872: pp 233 - 283.
- [8] GJ Czarnota, MC Kolios, H Vaziri, Ultrasound biomicroscopy of viable, dead and apoptotic cells.
Ultrasound in Med. and Biol. 1997: Vol. 23 pp. 961 - 965.
- [9] GJ Czarnota, MC Kolios, J Abraham, Ultrasound imaging of apoptosis: High-resolution noninvasive monitoring of programmed cell death in vitro, in situ and in vivo.
Br J Cancer 1999: pp 520 - 527.
- [10] A Tunis, GJ Czarnota, MC Kolios, Monitoring structural changes in cells with high frequency ultrasound signal statistics.
Ultrasound in Med. & Biol. 2005: Vol. 31 No. 8 pp 1041 – 1049.

- [11] R Vlad, S Brand, MC Kolios, GJ Czarnota, Quantitative ultrasound characterization of response to radiotherapy in cancer mouse models.
Clin Cancer Res 2009: pp 2067 - 2075
- [12] R Vlad, S Brand, MC Kolios, GJ Czarnota, Quantitative ultrasound characterization of cancer radiotherapy effect in vivo.
Int J Radiat Oncol Biol Phys 2008: 72: pp 1236 - 1243.
- [13] MC Kolios, GJ Czarnota, M Hussain, FS Foster, JW Hunt, MD Sherar, Analysis of ultrasound backscatter from ensembles of cells and isolated nuclei.
IEEE Ultrasonics Symposium 2001: pp 1257 - 1260.
- [14] FL Lizzi, M Greenebaum, EJ Feleppa, M Elbaum, DJ Coleman, Theoretical framework for spectrum analysis in ultrasonic tissue characterization.
Soc Am 1983: pp 1366 - 1373.
- [15] FL Lizzi, M Astor, EJ Feleppa, M Shao, A Kalisz, Statistical framework for ultrasonic spectral parameter imaging.
Ultrasound Med Biol 1997: 23: pp 1371 - 1382.
- [16] ML Oelze, WD O'Brien, JP Jr., Blue, JF Zachary, Differentiation and characterization of rat mammary fibroadenomas and 4T1 mouse carcinomas using quantitative ultrasound imaging.
IEEE Trans Med Imaging 2004: 23: pp 764 - 771.
- [17] EJ Feleppa, A Kalisz, S Melgar, Typing of prostate tissue by ultrasonic spectrum analysis.
IEEE Trans. Ultrason Ferroelec Freq Contr 1996: 43: pp 609 - 619.

[18] RH Silverman, R Folberg, MJ Rondeau, Spectral parameter imaging for detection of prognostically significant histologic features in uveal melanoma.

Ultrasound in Med. and Biol. 2003: 29: pp 951 - 959.

[19] FL Lizzi, DL King, MC Rorke, Comparison of theoretical scattering results and ultrasonic data from clinical liver examinations.

Ultrasound in Med. and Biol. 1988: 14: pp 377 - 385.

[20] N Lassau, M Lamuraglia, D Vanel, Doppler US with perfusion software and contrast medium injection in the early evaluation of isolated limb perfusion of limb sarcomas:

Prospective study of 49 cases.

Ann Oncol 2005: 16: pp 1054 - 1060.

[21] MC Kolios, GJ Czarnota, M Lee, JW Hunt, MD Sherar, Ultrasonic Spectral Parameter Characterization of Apoptosis

Ultrasound in Med. and Biol. 2002: Vol. 28, No. 5, pp. 589 - 597.

[22] R Vlad, Ph.D. Thesis, University of Toronto; 2008.

[23] A Tunis, D Spurrell, D McAlduff, A Giles, M Hariri, R Khokha, MD Sherar, GJ Czarnota, MC. Kolios, High frequency ultrasound signal statistics from mouse mammary tissue during involution.

IEEE Ultrasonics Ferroelec Control Symposium, Montreal, Canada, 2004: pp768 - 771.

[24] B Banihashemi, R Vlad, B Debeljevic, A Giles, MC Kolios, GJ Czarnota, Ultrasound Imaging of Apoptosis in Tumor Response: Novel Preclinical Monitoring of Photodynamic Therapy Effects

Cancer Res 2008; 68: pp 8590 - 8596.

[25] A Azrif, N Papanicolau, GJ Czarnota, Low frequency ultrasound detection of apoptotic cell death in-vitro and in-vivo.

Manuscript in preparation for publication

[26] PM Shankar, JM Reid, H Ortega, CW Piccoli, BB Goldberg, Use of non-rayleigh statistics for the identification of tumors in ultrasonic b-scans of the breast.

IEEE Trans Med Imaging 1993: 12: pp 687 - 692.

[27] PM Shankar, A model for ultrasonic scattering from tissues based on the k distribution.

Phys Med Biol 1995: 40: pp 1633 - 1649.

[28] PM Shankar, R Molthen, VM Narayanan, JM Reid, V Genis, F Forsberg, CW Piccoli, AE Lindenmayer, BB Goldberg, Studies on the use of non-rayleigh statistics for ultrasonic tissue characterization.

Ultrasound Med Biol 1996: 22(7): pp 873 - 882.

[29] PM Shankar, A compound scattering pdf for the ultrasonic echo envelope and its relationship to k and nakagami distributions.

IEEE Trans Ultrason Ferroelectr Freq Control 2003: 50(3): pp 339 - 343.

[30] PM Shankar, VA Dumane, JM Reid, V Genis, F Forsberg, C W Piccoli, BB Goldberg, Classification of ultrasonic b-mode images of breast masses using nakagami distribution.

IEEE Trans Ultrason Ferroelectr Freq Control 2001a: 48(2): pp 569 - 580.

[31] PM Shankar, VA Dumane, T George, CW Piccoli, JM Reid, F Forsberg, BB Goldberg, Classification of breast masses in ultrasonic b scans using nakagami and k distributions.

Phys Med Biol 2003b: 48(14): pp 2229 - 2240.

[32] BI Raju, MA Srinivasan, Statistics of envelope of high-frequency ultrasonic backscatter from human skin in vivo.

IEEE Trans Ultrason Ferroelectr Freq Control 2002: 49(7): pp 871 - 882.

[33] A Tuisi, M.A.S.C. Thesis, University of Toronto; 2005

[34] M Yaremko, FL Lizzi, EJ Fellepa, DJ Coleman, DL King , Two-dimensional power spectrum analysis for ultrasonic tissue characterization

IEEE Ultrasonics Symposium 1986: pp 933 - 936.

[35] DW Scott, On Optimal and Data-Based Histograms

Biometrika 1979: Vol. 66, No. 3, pp. 605 - 610.

[36] M Yang, TM Krueger, JG Miller, RM Holland, Characterization of anisotropic myocardial backscatter using spectral slope, intercept and midband fit parameters.

Ultrason Imaging 2007; pp 122 - 134.

[37] GJ Czarnota, R Karshafian, PN Burns, S Wong, J Lee, A Caissie, M Furukawa, AA Mahrouki, A Giles, Novel Ultrasound Induced Microbubble Enhancement of Radiation Response

Manuscript in preparation for publication

[38] EJ Feleppa, FL Lizzi, DJ Coleman, MM Yaremko, Diagnostic spectrum analysis in ophthalmology: a physical perspective.

Ultrasound Med Biol 1998: pp 623 - 631.

[39] ML Oelze, WD Jr. O'Brien, Method of improved scatterer size estimation and application to parametric imaging using ultrasound.

Acoust Soc Am 2002: pp 3053 - 3063.

[40] JW Hunt, AE Worthington, A Xuan, MC Kolios, GJ Czarnota, MD Sherar, A model based upon pseudo regular spacing of cells combined with the randomization of the nuclei can explain the significant changes in high-frequency ultrasound signals during apoptosis.

Ultrasound Med Biol 2002: 28: pp 217 - 226.

[41] FL Lizzi, M Astor, T Liu, C Deng, DJ Coleman, RH Silverman, Ultrasonic spectrum analysis for tissue assays and therapy evaluation.

Int J Imaging Syst Technol 1997: pp 3 - 10.

[42] K Jagdish, C Patel, CH Kapadia, and DB Owen, Handbook of statistical distributions.

Statistics, textbooks and monographs 1976: v20. M. Dekker, New York.

[42] RC Molthen, PM Shankar, F Forsberg, EJ Halpern, CW Piccoli, B Goldberg, Comparisons of the Rayleigh k-distribution models using in vivo breast and liver tissue. Ultrasound Med Biol, V24 1998: pp 93 - 100.

[43] Gnadt W, Manolakis D, Feleppa E, Liffi F, Liu T, Lee P, Classification of prostate tissue using neural networks

IEEE 1999: pp 3569 - 72.

[44] Lizzi FL, Ostromogilsky M, Fellepa EJ, Rork MC, Yaremko MM, Relationship of Ultrasonic Spectral Parameters to Features of Tissue Microstructure

IEEE Trans Ultrason Ferroelectr Freq Control 1986: UFFC-33.

[45] Dong F, Madsen EL, MacDonald MC, Zagzebski JA, Nonlinearity parameter for tissue-mimicking materials.

Ultrasound in Med. Biol 1999: 25: pp 831 - 838.

②
Bk-61-183